

The Atmospherically Important Reaction of Hydroxyl Radicals with Methyl Nitrate: A Theoretical Study involving the Calculation of Reaction Mechanisms, Enthalpies, Activation Energies and Rate Coefficients

Maggie Ng, Daniel K.W. Mok, Edmond P. F. Lee, and John M. Dyke

J. Phys. Chem. A, **Just Accepted Manuscript** • DOI: 10.1021/acs.jpca.7b05035 • Publication Date (Web): 09 Aug 2017

Downloaded from <http://pubs.acs.org> on August 25, 2017

Just Accepted

“Just Accepted” manuscripts have been peer-reviewed and accepted for publication. They are posted online prior to technical editing, formatting for publication and author proofing. The American Chemical Society provides “Just Accepted” as a free service to the research community to expedite the dissemination of scientific material as soon as possible after acceptance. “Just Accepted” manuscripts appear in full in PDF format accompanied by an HTML abstract. “Just Accepted” manuscripts have been fully peer reviewed, but should not be considered the official version of record. They are accessible to all readers and citable by the Digital Object Identifier (DOI®). “Just Accepted” is an optional service offered to authors. Therefore, the “Just Accepted” Web site may not include all articles that will be published in the journal. After a manuscript is technically edited and formatted, it will be removed from the “Just Accepted” Web site and published as an ASAP article. Note that technical editing may introduce minor changes to the manuscript text and/or graphics which could affect content, and all legal disclaimers and ethical guidelines that apply to the journal pertain. ACS cannot be held responsible for errors or consequences arising from the use of information contained in these “Just Accepted” manuscripts.

1
2
3
4
5
6
7
8
9
10
11
12
13
14
15
16
17
18
19
20
21
22
23
24
25
26
27
28
29
30
31
32
33
34
35
36
37
38
39
40
41
42
43
44
45
46
47
48
49
50
51
52
53
54
55
56
57
58
59
60

**The Atmospherically Important Reaction of Hydroxyl Radicals with
Methyl Nitrate: A Theoretical Study involving the Calculation of Reaction
Mechanisms, Enthalpies, Activation Energies and Rate Coefficients.**

by

Maggie Ng,^a Daniel K. W. Mok,^a Edmond P. F. Lee,^{*,a,b} and John M. Dyke^{*,b}

a Department of Applied Biology and Chemical Technology, Hong Kong Polytechnic University, Hung Hom, Hong Kong.

b School of Chemistry, University of Southampton, Southampton SO17 1BJ, U.K. emails:
epl@soton.ac.uk; jmdyke@soton.ac.uk

Abstract

A theoretical study, involving the calculation of reaction enthalpies and activation energies, mechanisms and rate coefficients, has been made of the reaction of hydroxyl radicals with methyl nitrate, an important process for methyl nitrate removal in the earth's atmosphere.

Four reaction channels were considered:- formation of $\text{H}_2\text{O} + \text{CH}_2\text{ONO}_2$, $\text{CH}_3\text{OOH} + \text{NO}_2$, $\text{CH}_3\text{OH} + \text{NO}_3$, and $\text{CH}_3\text{O} + \text{HNO}_3$. For all channels, geometry optimization and frequency calculations were carried out at the M06-2X/6-31+G** level, while relative energies were improved at the UCCSD(T*)-F12/CBS level. The major channel is found to be the H abstraction channel, to give the products $\text{H}_2\text{O} + \text{CH}_2\text{ONO}_2$. The reaction enthalpy ($\Delta H_{298\text{K}}^{\text{RX}}$) of this channel is computed as $-17.90 \text{ kcal.mol}^{-1}$. Although the other reaction channels are also exothermic, their reaction barriers are high ($> 24 \text{ kcal.mol}^{-1}$) and therefore these reactions do not contribute to the overall rate coefficient in the temperature range considered (200-400 K). Pathways via three transition states have been identified for the H abstraction channel. Rate coefficients were calculated for these pathways at various levels of variational transition state theory (VTST) including tunneling. The results obtained are used to distinguish between two sets of experimental rate coefficients, measured in the temperature range 200-400K, one of which is approximately an order of magnitude greater than the other. This comparison, as well as the temperature dependence of the computed rate coefficients, shows that the lower experimental values are favoured. The implications of the results to atmospheric chemistry are discussed.

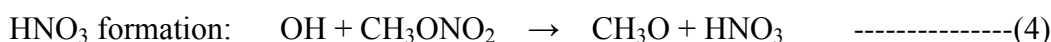
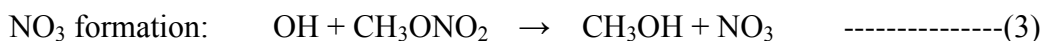
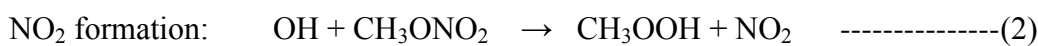
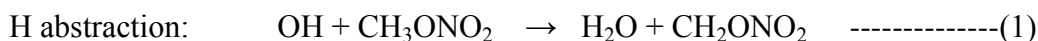
Introduction

Alkyl nitrates act as temporary reservoirs of nitrogen oxide radicals in the lower atmosphere (the troposphere) as they have relatively long atmospheric lifetimes, of the order of days to weeks^{1,2}. This enables them to undergo long-range transport to remote areas where they can release NO_x (defined here as NO + NO₂ + NO₃) that can give rise to ozone formation. As a result, alkyl nitrates play an important role in contributing to the concentration of O₃ in the troposphere. Methyl nitrate (CH₃ONO₂) and ethyl nitrate (C₂H₅ONO₂) are present in the troposphere mainly from marine emissions³⁻⁶ whereas larger alkyl nitrates are predominantly produced through atmospheric oxidation of hydrocarbons in the presence of NO_x (*e.g.* in urban or polluted areas)¹⁻⁷. CH₃ONO₂ and C₂H₅ONO₂ account for 20-40% of the light (C_n ≤ 5) alkyl nitrates in the troposphere with concentrations of 1-43 pptv and 1-50 pptv respectively having been measured^{3,6,8}. For the heavier alkyl nitrates, with 4 or more carbon atoms, the association reaction of NO with RO₂ becomes a significant alkyl nitrate source *i.e.* RO₂ + NO + M → RONO₂ + M (M is a third body), whereas for C_n ≤ 4 the major product channel from the RO₂ + NO reaction is RO + NO₂.

A number of recent regional and global model studies have demonstrated that key kinetic and photolytic parameters for alkyl nitrates are missing, preventing chemical models from describing their atmospheric oxidation chemistry adequately and hence obtaining their atmospheric lifetimes (9,10). These parameters include their loss rate via reaction with OH and O₃, and whether NO_x is released in these reactions. Also, how much NO_x (photochemically reactive nitrogen oxide) and how much HNO₃ (photochemically non-reactive nitrogen oxide) are eventually formed from organic nitrate reactions is important in understanding the contribution of alkyl nitrates to the oxidizing capacity of the troposphere⁸. In a recent study of the mechanism of the atmospherically relevant reaction of chlorine atoms with methyl nitrate and calculation of the rate coefficient of this reaction at temperatures relevant to the troposphere¹¹, we noted that the lifetime of methyl nitrate in the troposphere is determined by loss through photolysis, reaction with OH and reaction with Cl atoms. This is because methyl nitrate is thermally stable in the troposphere in the temperature range 200-300 K and heterogeneous removal is slow because its solubility in and reactivity with water is low. The photolysis rate of CH₃ONO₂ in the atmosphere has been determined on a number of occasions^{12,13} and the rate coefficient (*k*) of the Cl + CH₃ONO₂ reaction is now reliably known in the temperature range 200-300 K¹¹. However, the rate coefficient of the OH +

CH₃ONO₂ reaction in this temperature range is not well established. Available experimental rate coefficients at 298 K occur in two groups which differ by an order of magnitude, a lower group at $\sim 3 \times 10^{-14}$ cm³ molecule⁻¹ s⁻¹ ¹⁴⁻¹⁷ and a higher group at $\sim 3 \times 10^{-13}$ cm³ molecule⁻¹ s⁻¹ ^{18,19}. There is also uncertainty over the temperature dependence of this rate coefficient. Nielsen et al. ¹⁸ report a value of $(3.2 \pm 0.5) \times 10^{-13}$ cm³ molecule⁻¹ s⁻¹ at 298 K and a negative temperature dependence of k in the region 298-393 K, whereas Shallcross et al. ¹⁵ and Talukdar et al. ¹⁴ report 298 K values of $(2.33 \pm 0.14) \times 10^{-14}$ cm³ molecule⁻¹ s⁻¹ and $(4.7 \pm 1.0) \times 10^{-14}$ cm³ molecule⁻¹ s⁻¹ respectively and a positive temperature dependence in the region 220-420 K. Also, Talukdar et al. ¹⁴ suggest that the OH + CH₃ONO₂ reaction proceeds via H abstraction, based on the fact that the measured rate coefficient was independent of gas composition, the observed trend of rate coefficients as the size of the alkyl group is increased and the large observed primary kinetic isotope effect (as seen in the ratio of the k 's measured for OH + CH₃ONO₂ vs OH + CD₃ONO₂). However, the mechanism of the reaction is not well established

In this work, the following reaction channels were considered



Using available heats of formation ($\Delta H_{f,298\text{K}}$) of the respective reactants/products, the enthalpies of these reactions, $\Delta H_{298\text{K}}^{\text{RX}}$, were evaluated as $\Delta H_1 = -17.72$ kcal.mol⁻¹, $\Delta H_2 = -2.41$ kcal.mol⁻¹, $\Delta H_3 = -9.83$ kcal.mol⁻¹, $\Delta H_4 = -7.22$ kcal.mol⁻¹ (see Tables 1, 2, 4-7; *vide infra*).

CH₃ONO₂ has a C_s structure with the methyl group staggered with respect to the cis oxygen of the NO₂ group ²⁰. The methyl V₃ rotational barrier is 811 cm⁻¹. In the CH₃ group, one hydrogen atom is in the plane of the heavy atoms, trans to the O-N bond of the C-O-N unit, while the other two hydrogen atoms lie above and below the plane respectively.

The aim of this work is to use state-of-the-art wavefunction and DFT methods to investigate the reaction mechanisms of these OH + CH₃ONO₂ reactions and to compute reaction rate coefficients in the 200-400 K region which should be valuable to test the available experimental values and to decide which experimental values are the more reliable.

Theoretical considerations and computational details

Ab initio and DFT calculations

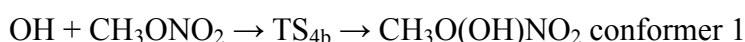
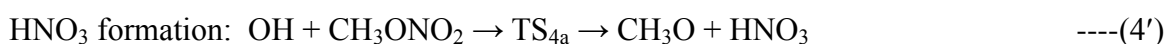
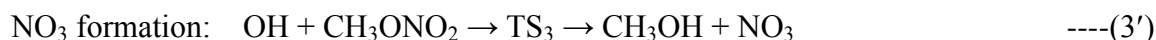
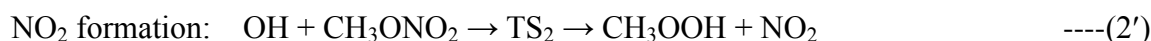
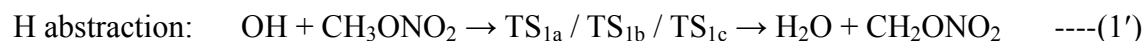
Geometry optimization, transition state (TS) search, intrinsic reaction coordinate (IRC) and vibrational frequency calculations were carried out using the M06-2X functional²¹ and the 6-31+G** basis set with the Gaussian 09 suite of programs²². The M06-2X functional was chosen because it has been shown to perform particularly well for TS structures and reaction barrier heights in some recent benchmark studies²³⁻²⁶. It is a highly parameterised hybrid meta functional which allows for mid-range interactions but not dispersion. It is recommended in refs (23-26) for calculations of main group thermochemistry, kinetics and non-covalent interactions. In the IRC calculations, using the Hessian-based predictor-corrector (HPC) reaction path following method²⁷⁻²⁹, 15 points from the TS in each direction towards the reactants and products were computed with a step size of 0.1 bohr, and gradients and Hessians were calculated analytically at every IRC point. The computed IRC paths of all the reaction channels cover reaction coordinates of up to *ca. s* = ±1.50 bohr.

Electronic energies of the reactants, products, TSs, reactant complexes (RCs) and product complexes (PCs) were improved by performing single-point energy calculations with the explicitly correlated UCCSD(T*)-F12x (where x = a or b) methods^{30,31} on the geometries optimized at the M06-2X/6-31+G** level using the MOLPRO suite of programs^{32,33}. The VTZ-F12 and VQZ-F12 basis sets³⁴ were employed for the atomic orbital (AO) basis sets. The corresponding AVXZ/MP2FIT³⁵ basis sets (X = T or Q) were used to compute the F12 integrals by density fitting (DF) while the VXZ-F12/OPTRI³⁴ basis sets were used to compute the many electron integrals by the resolution of identity (RI) method. The computed UCCSD(T*)-F12x/VTZ-F12 and UCCSD(T*)-F12x/VQZ-F12 relative electronic energies, with respect to the separate reactants, were extrapolated to the complete basis set (CBS) limit employing two schemes. In the first scheme, the two-point $1/X^3$ formula of Helgaker et al.^{36,37} was used to extrapolate the relative electronic energies computed at the UCCSD(T*)-F12x/VTZ-F12 and UCCSD(T*)-F12x/VQZ-F12 levels, and the extrapolated relative electronic energies are denoted as CBS1. In the other scheme, the relative electronic energies computed at the UCCSD(T*)-F12x/VTZ-F12 and UCCSD(T*)-F12x/VQZ-F12 levels were extrapolated to the CBS limit by the generalized formula of Schwenke³⁸, with the CBS coefficients optimized by Hill et al.³⁹ for CCSD-F12b energies with the VTZ-F12/VQZ-F12 basis set combination. The extrapolated relative electronic energies thus obtained are denoted as CBS2. The averages of the computed UCCSD(T*)-F12a/CBS1//M06-2X/6-31+G**,
60

UCCSD(T*)-F12b/CBS1//M06-2X/6-31+G**, UCCSD(T*)-F12a/CBS2//M06-2X/6-31+G** and UCCSD(T*)-F12b/CBS2//M06-2X/6-31+G** relative electronic energies, labelled as UCCSD(T*)-F12ave/CBSave//M06-2X, are considered to be the best theoretical estimates in the present study. The choice of the average value as the best theoretical estimate is mainly because the values obtained by the various extrapolation schemes described above are very close to each other (*vide infra*).

In the $^2\Pi$ state of OH, the spin-orbit (SO) splitting of 139.6 cm^{-1} results in an energy lowering of the unperturbed $^2\Pi$ state to the $^2\Pi_{3/2}$ state of $0.20\text{ kcal mol}^{-1}$ ⁴⁰. Therefore, all the computed relative energies, namely, reaction enthalpies ($\Delta H_{298\text{K}}^{\text{RX}}$), reaction energies (ΔE^{RX}) and activation energies (ΔE^\ddagger), were increased by $0.20\text{ kcal mol}^{-1}$ to allow for this. This correction has also been applied to the relative energy of the RCs and PCs, notably for reaction 1. Also, the electronic partition functions of both the $^2\Pi_{3/2}$ and $^2\Pi_{1/2}$ states of OH, together with the appropriate energies and degeneracies, were included in the subsequent rate coefficient calculations.

For reactions (1)-(4), the transition states that were located in the M06-2X calculations can be labelled as follows (*vide infra*):-



Rate coefficient calculations

Reaction rate coefficients were computed for the H abstraction channel {channel (1)} at various TST levels in single-level and improved single-level direct dynamics calculations at temperatures in the region 200-400 K using the POLYRATE 2010-A program⁴¹. The rate coefficients obtained correspond to rate coefficients obtained in the high pressure limit. As the computed barrier heights of channels (2), (3) and (4) are considerably higher than that of channel (1), only channel (1) was considered in the rate coefficient calculations. In addition, for channel (1), the computed energies of TS_{1b} and TS_{1c} relative to the reactants are higher than that of TS_{1a} by *ca.* 2-3 kcal mol^{-1} and therefore it is expected that TS_{1a} would contribute

1
2
3
4 the most to the total rate coefficient of channel (1).

5 The geometries of the reactants, reactant complex (RC), TS, product complex (PC),
6 products and the 30 non-stationary points on the IRC path obtained at the M06-2X/6-31+G**
7 level, together with the corresponding analytical gradients and Hessians, were used in the
8 single-level direct dynamics calculations. All the methyl torsional modes (in CH₃ONO₂ and
9 the RC) were treated as hindered internal rotations within the hindered-internal-rotator (HIR)
10 approximation⁴² using the full Chuang-Truhlar (CT) method^{43,44}. The V_{MEP} curves were
11 obtained by interpolation/extrapolation in the range of $s = \pm 0.86 \text{ \AA}$ using the Euler-steepest-
12 descents (ESD) method⁴⁵ with a Hessian step size of $2.39 \times 10^{-3} \text{ \AA}$, which is nine times larger
13 than the gradient step size of $2.65 \times 10^{-4} \text{ \AA}$. In the generalized normal mode analysis,
14 curvilinear internal coordinates⁴⁶ were used instead of the redundant internal coordinates⁴⁷
15 because it was found in the present study that the redundant internal coordinates gave extra
16 imaginary vibrational frequencies, which indicate unphysical descriptions of the vibrational
17 motions of the molecules. With curvilinear internal coordinates, no extra imaginary
18 vibrational frequency was found along the minimum energy path (MEP). Rate coefficients
19 were calculated at different TST levels, namely, conventional transition state theory (TST),
20 canonical variational transition state theory (CVT) and improved canonical variational
21 transition state theory (ICVT), with different tunneling methods, including zero-curvature
22 tunneling (ZCT) and small-curvature tunneling (SCT) corrections.

23
24
25
26
27
28
29
30
31
32
33
34
35
36
37 Improved single-level direct dynamics calculations⁴⁸ were carried out, with the M06-
38 2X/6-31+G** V_{MEP} curve as the lower level (LL) and the higher-level (HL) V_{MEP} curve
39 obtained by using the computed HL energies of five stationary points. These are the
40 separated reactants, RC, TS, PC and the separated products computed at the UCCSD(T*)-
41 F12ave/CBSave level (the average of the four CBS values). More IRC points on the HL V_{MEP}
42 were obtained by the following scaling expression devised by us previously (equation (5),⁴⁹).

$$43 \quad E_s^{HL} = (E_s^{LL} - E_{RC}^{LL}) \cdot \{(E_{TS}^{HL} - E_{RC}^{HL}) / (E_{TS}^{LL} - E_{RC}^{LL})\} + E_{RC}^{HL} \quad (5)$$

44
45
46
47
48
49
50
51
52
53
54
55
56
57
58
59
60
With this expression, an improved HL energy (E_s^{HL}) at a certain s along the LL IRC can be
evaluated using the LL energy (E_s^{LL}) and the ratio between the computed HL and LL barriers.
Together with the HL energies of the five stationary points, the additional HL IRC energies
obtained from this scaling expression were used in improved single-level rate coefficient
calculations with the geometries and vibrational frequencies at the lower level. This scaling
formula gave almost identical rate coefficients as those obtained with the dual-level mapping
method of POLYRATE⁴⁸ (more detail is given in the Supplementary Information section
SII).

Results and discussion

Ab initio and DFT results

From the results of the *ab initio* and DFT calculations, channels (2), (3) and (4) were found to have considerably higher barrier heights ($> 20 \text{ kcal mol}^{-1}$) than channel (1). As a result, channel (1) is the dominant pathway of the $\text{OH} + \text{CH}_3\text{ONO}_2$ reaction and will be considered, after channels (2), (3) and (4) have been discussed. The contributions of channels (2), (3) and (4) to the total rate coefficient of the $\text{OH} + \text{CH}_3\text{ONO}_2$ reaction are expected to be negligibly small and hence they were neglected in the subsequent rate coefficient calculations.

Inspection of the results of UCCSD(T*)-F12x calculations shows that the effects of basis set size on the computed ΔE_e^{RX} and ΔE_e^{\ddagger} (the reaction energy and activation energy respectively calculated using only electronic energies), the energy differences between the F12a and F12b results, and those between the two CBS extrapolation schemes (CBS1 and CBS2) are small in all channels, as the energy differences are within chemical accuracy (1 kcal. mol^{-1}). The geometries of the TSs in all channels (equations 1'-4'), optimized at the M06-2X/6-31+G** level, are shown in Figure 1, while those of the adduct conformers in channel (4) and those of the RC and PC in channel (1) are shown in Figure 2. Furthermore, the $\Delta E_{0\text{K}}$ values computed at the UCCSD(T*)-F12ave/CBSave//M06-2X level are summarized in the energy profile in Figure 3.

NO_2 formation: $\text{OH} + \text{CH}_3\text{ONO}_2 \rightarrow \text{CH}_3\text{OOH} + \text{NO}_2$ --- Channel (2)

The geometry of the TS in channel (2'), TS_2 , optimized at the M06-2X/6-31+G** level is shown in Figure 1. The computed imaginary vibrational frequency of TS_2 , $988i \text{ cm}^{-1}$, corresponds to the asymmetric O...O...N stretching mode, indicating that TS_2 undergoes O-N bond breaking and O-O bond formation via a $\text{S}_{\text{N}}2$ mechanism to release NO_2 , when the O atom of the OH radical attacks the O atom next to the methyl group. In TS_2 , the breaking C-N bond is elongated by 33% while the forming O-O bond is longer than that in CH_3OOH by 22%. Hence, it is not obvious whether TS_2 is reactant-like or product-like, as the elongations of the breaking C-N bond and the forming O-O bond are comparable. The computed reaction energies (ΔE_e^{RX}) and activation energies (ΔE_e^{\ddagger}) of channel (2) at various levels of theory are summarized in Table 1. The best computed ΔE_e^{RX} and ΔE_e^{\ddagger} values (labelled as F12ave/CBSave) are -1.72 ± 0.01 and $24.08 \pm 0.17 \text{ kcal mol}^{-1}$. Including the zero-point

energy (ZPE) correction and the spin-orbit correction for OH, the best computed ΔE_{0K}^{RX} and ΔE_{0K}^{\ddagger} values of -1.21 and 24.56 kcal mol⁻¹ are obtained. This indicates that channel (2) has a high activation barrier and, therefore, its contribution to the total rate coefficient of the OH + CH₃ONO₂ reaction is negligible (more detail is given in the Supplementary Information section SI2).

NO₃ formation: OH + CH₃ONO₂ → CH₃OH + NO₃ --- Channel (3)

The geometry of the TS in channel (3'), TS₃, optimized at the M06-2X/6-31+G** level is shown in Figure 1. The imaginary vibrational frequency of 1251i cm⁻¹ corresponds to the asymmetric O...C...O stretching mode, which shows that TS₃ undergoes O-C bond breaking and C-O bond forming via a S_N2 mechanism to release NO₃ when the O atom in the OH radical attacks the C atom in the methyl group. The breaking O-C bond in TS₃ is elongated by 29% while the forming C-O bond is longer than the equilibrium value of 1.41 Å in CH₃OH by 25%, and so the TS₃ is not reactant-like or product-like. The computed ΔE_e^{RX} and ΔE_e^{\ddagger} values at various levels of theory are summarized in Table 2. The best computed ΔE_e^{RX} and ΔE_e^{\ddagger} values at the F12ave/CBSave level are -7.99 ± 0.12 and 36.07 ± 0.11 kcal mol⁻¹ respectively, and the corresponding best computed ΔE_{0K}^{RX} and ΔE_{0K}^{\ddagger} values are -7.73 and 37.09 kcal mol⁻¹. Although the computed ΔH_{298K}^{RX} value of -8.01 kcal mol⁻¹ indicates that channel (3) is exothermic, the large reaction barrier height of 37.09 kcal mol⁻¹ means that this reaction will only make an extremely small contribution to the overall OH + CH₃ONO₂ rate coefficient. As a result, channel (3) was also not considered in the rate coefficient calculations (more detail is given in the Supplementary Information section SI3).

HNO₃ formation: OH + CH₃ONO₂ → CH₃O + HNO₃ --- Channel (4)

The reaction leading to HNO₃ formation can take place through a concerted mechanism, in which the reactants proceed to the products via a transition state, or through a stepwise mechanism involving adduct formation (see equation 4'). Both pathways are calculated to have high activation energies (> 28 kcal.mol⁻¹) and therefore this channel is not expected to contribute to the overall reaction rate coefficient (more detail is given in the Supplementary Information section SI4).

H abstraction: OH + CH₃ONO₂ → H₂O + CH₂ONO₂ --- Channel (1)

In channel (1), a H atom of the methyl group of CH₃ONO₂ is abstracted by the OH

radical to give H₂O and CH₂ONO₂. As shown in equation (1'), three TS's have been located and their optimized geometries at the M06-2X/6-31+G** level are shown in Figure 1. Some major geometrical parameters, the imaginary vibrational frequencies, the ΔE_e and ΔE_{0K} values as well as the ZPE corrections of the three TS's are summarized in Table 6. In TS_{1a} and TS_{1b}, the OH radical abstracts the out-of-plane H atom, with the O-H bond in the OH radical nearly parallel to the C_s plane of CH₃ONO₂. The geometry of TS_{1a} is similar to that of TS_{1b}, except that in TS_{1a} the H atom in the OH radical points towards the O atom in the nitrate group and this results in a O---H hydrogen bond-like interaction with a distance of 2.34 Å between the O and H atoms. In TS_{1c}, the OH radical abstracting the in-plane H atom is in the C_s plane of CH₃ONO₂, and the O-H bond in the OH radical is almost parallel to the C-O bond. TS_{1a}, TS_{1b} and TS_{1c} have imaginary vibrational frequencies of 1294i, 1135i and 1486i cm⁻¹ respectively (see Table 6), which correspond to the asymmetric C...H...O stretching mode. The *L* parameters determined from the ratio of the elongation of the breaking C-H bond to that of the forming H-O bond $\{L = \Delta(C-H)/\Delta(H-O)\}$ are 0.39, 0.25 and 0.39 for TS_{1a}, TS_{1b} and TS_{1c} respectively, indicating that all the three TS's are reactant-like because their *L* parameters are smaller than 1. It can be seen that both the ΔE_e and the ΔE_{0K} values of the TS's are in the order TS_{1c} > TS_{1b} > TS_{1a}. TS_{1a} has the lowest energy of the three TS's, as expected, due to the presence of the hydrogen bond-like interaction, which stabilizes TS_{1a} by *ca.* 1.5 to 2 kcal mol⁻¹. The best computed activation energies (ΔE_e without ZPE and OH spin-orbit corrections) to the transition states TS_{1a}, TS_{1b} and TS_{1c}, at the F12ave/CBSave level, are 4.02, 5.52 and 7.05 kcal mol⁻¹ respectively. They are within 1 kcal.mol⁻¹ of the corresponding M06-2X values (3.01, 5.10 and 6.23 kcal.mol⁻¹), suggesting that the M06-2X functional performs well for barrier heights of this channel, especially for TS_{1b} where the energy difference between the M06-2X and the F12ave/CBSave levels is 0.42 kcal mol⁻¹. With the ZPE and spin-orbit corrections, the best computed activation energies (ΔE_{0K}) associated with TS_{1a}, TS_{1b} and TS_{1c} are 2.76, 4.02 and 5.04 kcal mol⁻¹ respectively, showing that channel (1) has the lowest barrier height of all channels and hence is the dominant pathway of the OH + CH₃ONO₂ reaction. This supports the conclusion of the study of Talukdar *et al.*¹⁴ that the OH + alkyl nitrate reaction proceeds via simple H abstraction, rather than OH addition suggested by He *et al.*⁸.

Regarding the out-of-plane OH + CH₃ONO₂ → H₂O + CH₂ONO₂ channel via TS_{1a}, a RC and a PC (labelled as RC_{1a} and PC_{1a} respectively) have been located in the entrance and exit channels respectively. The geometries of the RC_{1a} and PC_{1a} optimized at the M06-2X/6-

31+G** level are shown in Figure 2. In the seven-membered ring RC_{1a}, there is an interaction between the H atom of the OH radical and the O atom in the nitrate group with a O---H distance of 2.51 Å. In PC_{1a}, the two H atoms in H₂O are oriented to enable interactions with the two O atoms in the nitrate group with O---H distances of 2.96 Å and 3.25 Å. The computed ΔE_e , ΔE_{0K} and ΔH_{298K} values of the RC_{1a} and PC_{1a}, together with those of TS_{1a} and the separate products, obtained at various UCCSD(T*)-F12x//M06-2X/6-31+G** levels are summarized in Table 7. These values were used in the rate coefficient calculations with POLYRATE. The energies of the RC_{1a} and PC_{1a} are lower than the separate reactants and products, respectively, by *ca.* 3 kcal mol⁻¹. The best computed ΔE_e values of the RC_{1a}, TS_{1a}, PC_{1a} and the separate products at the F12ave/CBSave level are -3.01 ± 0.01 , 4.02 ± 0.05 , -20.51 ± 0.07 and -17.23 ± 0.08 kcal mol⁻¹ respectively. The estimated uncertainties are within 0.1 kcal mol⁻¹, which are negligibly small, for all the species. It was found that the M06-2X functional performs reasonably well for the ΔE_e values of TS_{1a} and PC_{1a}, and fairly well for the ΔE_e values of RC_{1a} and the separate products, as the differences between the M06-2X and the F12ave/CBSave values for RC_{1a}, TS_{1a}, PC_{1a} and separate products are 2.41, 1.03, 0.20 and 2.64 kcal mol⁻¹ respectively. The best computed ΔH_{298K}^{RX} value (including the spin-orbit correction) for channel (1) is -17.90 kcal mol⁻¹, which is lower than the ΔH_{298K}^{RX} of -13.92 kcal mol⁻¹ evaluated from the available $\Delta H_{f,298K}$ values of CH₃ONO₂⁵⁰, OH⁵¹, CH₂ONO₂⁵⁰, and H₂O⁵² by *ca.* 4 kcal mol⁻¹. However, it agrees very well with the ΔH_{298K}^{RX} value of -17.72 kcal mol⁻¹ determined using these $\Delta H_{f,298K}$ values but with the $\Delta H_{f,298K}$ values for CH₃ONO₂ and CH₂ONO₂, obtained from the tabulation of Burcat et al.⁵⁰, replaced by -29.71 and 19.30 kcal mol⁻¹ respectively, computed in our previous study¹¹.

Rate coefficients of the OH + CH₃ONO₂ → H₂O + CH₂ONO₂ channel

Computed rate coefficients at the M06-2X single level

The reaction paths, including the V_{MEP} , ΔZPE and V_a^G curves, obtained at the M06-2X/6-31+G** level for the OH + CH₃ONO₂ → H₂O + CH₂ONO₂ C-H out-of-plane channel via TS_{1a} are shown in Figure 4 (upper panel). There is a dip of ~ 3 kcal mol⁻¹ in the ΔZPE curve near the saddle point region ($s = 0$), which leads to a shift of the maximum of the V_a^G curve to $s = -0.16$ Å. The computed rate coefficients for this channel (k_{1a}), obtained at different VTST levels using the M06-2X IRC, plotted against temperature are shown in Figure 5. The available experimental values¹⁴⁻¹⁹ determined in the temperature range of 200-423 K are also included in the lower part of this figure ($\log_{10}k$ vs $1000/T$). It should be noted

1
2
3
4
5
6
7
8
9
10
11
12
13
14
15
16
17
18
19
20
21
22
23
24
25
26
27
28
29
30
31
32
33
34
35
36
37
38
39
40
41
42
43
44
45
46
47
48
49
50
51
52
53
54
55
56
57
58
59
60

that all the k_{1a} computed rate coefficients have been multiplied by two to account for the two possible C-H out-of-plane H abstraction sites, which are equivalent. The higher sets of experimental values from Nielsen et al.¹⁸ and Kerr et al.¹⁹ are not shown in the upper part of Figure 5, the k vs T plot, as they are considerably larger than the other values. They are however shown in the lower part of Figure 5 where $\log_{10}k$ is the vertical axis. As expected, the computed TST rate coefficients, k^{TST} , at a given temperature are larger than all the VTST computed values. They are larger than the CVT and ICVT values by an order of magnitude, indicating that the variational effect is significant. The tunneling effects, whether with ZCT or SCT, are small when $T > 360$ K, as the transmission coefficients are close to unity. However, the tunneling effects become more significant as temperature decreases. The transmission coefficients with ZCT and SCT at 200 K are 4.56 and 9.64 respectively; thus the SCT correction at this temperature can increase the computed rate coefficients by nearly an order of magnitude. The classical adiabatic ground-state (CAG) correction⁵³⁻⁵⁵ accounts for the fact that the generalized transition state (GTS) at the CVT level is not located at the maximum of the V_a^G curve. The CAG factor at the CVT level ($\kappa^{\text{CVT/CAG}}$) is close to unity in the range 200-400 K, indicating that the CAG correction with CVT is insignificant, because the maximum of the ΔG curve is located at $s \approx -0.15$ Å, which is near to the maximum of the V_a^G curve ($s = -0.16$ Å). (ΔG is the change in free energy of the reaction system relative to the reactants). Considering the computed rate coefficients at the highest ICVT/SCT level ($k^{\text{ICVT/SCT}}$), they are closer to the lower sets of experimental values of Gaffney et al.¹⁶, Talukdar et al.¹⁴, Kakesu et al.¹⁷ and Shallcross et al.¹⁵, than the higher values of Nielsen et al.¹⁸ and Kerr et al.¹⁹, but are lower than the lower group of experimental values by an order of magnitude. In addition, the computed $k^{\text{ICVT/SCT}}$ values show a positive temperature dependence which is observed in the lower set of experimental values but not in the higher group, indicating that the computed $k^{\text{ICVT/SCT}}$ values, derived from the computed M06-2X reaction paths, favour the lower set of experimental values.

Computed rate coefficients at the UCCSD(T*)-F12ave/CBSave//M06-2X/6-31+G** dual level

The V_{MEP} , ΔZPE and V_a^G curves obtained at the UCCSD(T*)-F12ave/CBSave//M06-2X/6-31+G** level for the $\text{OH} + \text{CH}_3\text{ONO}_2 \rightarrow \text{H}_2\text{O} + \text{CH}_2\text{ONO}_2$ C-H out-of-plane channel via TS_{1a} are shown in Figure 4 (lower panel). As shown in Table 7, ΔE_e^\ddagger obtained at the UCCSD(T*)-F12ave/CBSave//M06-2X/6-31+G** level is 4.02 kcal.mol⁻¹ compared with 3.01 kcal.mol⁻¹ at the M06-2X/6-31+G** level (both values are without correction for OH

spin-orbit splitting which would increase them both by 0.20 kcal.mol⁻¹). The HL V_{MEP} and V_{a}^{G} curves are shown in the lower half of Figure 4. These were obtained using HL energies of the reactants, RC_{1a}, TS_{1a}, PC_{1a} and products, as well as extra HL IRC points calculated by the expression devised by us previously (equation (5) and ref.(49)). The HL F12ave/CBSave V_{MEP} curve follows the shape of the M06-2X V_{MEP} curve and has a maximum of 4.22 kcal mol⁻¹ at $s = 0$. The plots of the rate coefficients computed at various VTST levels for this channel (1(a)) with the HL F12ave/CBSave//M06-2X/6-31+G** IRC in the temperature range between 200 K and 400 K are shown in Figure 6. The spread and the order of the F12ave/CBSave k values at different VTST levels are similar to those of the M06-2X k values. However, the F12ave/CBSave k values are smaller than the corresponding M06-2X values by an order of magnitude, as the F12ave/CBSave ΔE^{\ddagger} is higher than the M06-2X ΔE^{\ddagger} by *ca.* 1 kcal mol⁻¹. Computed ICVT/SCT rate coefficients of reactions (1a), (1b) and (1c) in the temperature range between 200 K and 400 K, as well as the total rate coefficients of the hydrogen atom abstraction reaction, obtained with the HL F12ave/CBSave//M06-2X/6-31+G** IRC, are shown in Figure 7 (see also Tables SI5 and SI6 in the Supplementary Information (SI)). The total rate coefficient has been obtained from $k_{\text{total}} = 2k_{1\text{a}} + 2k_{1\text{b}} + k_{1\text{c}}$, as there are two hydrogen atoms in CH₃ONO₂ that could be removed in channels 1a and 1b (the out-of-plane H atoms), but only one that could be removed in channel 1c (the in-plane H atom). This figure shows that $k_{1\text{a}}$ is the main contribution to the overall rate coefficient in the temperature range 200-300K, with $k_{1\text{b}}$ also becoming significant above 300 K. $k_{1\text{c}}$ is significantly lower than $k_{1\text{a}}$ by at least an order of magnitude at all temperatures considered, and hence its contribution to $k(\text{total})$ is very small. As can be seen from Figure 7, $k_{1\text{b}}$ becomes comparable with $k_{1\text{a}}$ at temperatures higher than 280 K, and $k_{1\text{b}}$ becomes higher than $k_{1\text{a}}$ at temperatures greater than 334K ($1000/T = 2.99 \text{ K}^{-1}$). This is somewhat surprising as channel 1b has a higher barrier than channel 1a ($\Delta E_{\text{e}}^{\ddagger}$ values 4.22 (1a) and 5.72 (1b) kcal.mol⁻¹ respectively). This arises because the entropy term (ΔS^{\ddagger}) in the rate coefficient (ΔS^{\ddagger} is negative in both cases) makes a larger contribution to $k_{1\text{b}}$ than $k_{1\text{a}}$ in the temperature range 340-400 K, such that ΔG^{\ddagger} is more positive for channel 1a than 1b in the temperature range 340-400 K, whereas ΔG^{\ddagger} is less positive for channel 1a than 1b in the temperature range 200-340 K.

The computed $k^{\text{ICVT/SCT}}$ values of channel 1 (k_{total}) at the F12ave/CBSave level fall below the experimental values, indicating that the F12ave/CBSave $\Delta E_{\text{e}}^{\ddagger}$ for TS_{1a} of 4.22 kcal mol⁻¹ and $\Delta E_{\text{e}}^{\ddagger}$ for TS_{1b} of 5.72 kcal mol⁻¹ (with spin-orbit correction of OH) are too high (see

1
2
3 Table 8; the $k^{\text{ICVT/SCT}}$ values are shown in column 3). In order to obtain an improved match
4 between theory and experiment, calculations were carried out with reduced barrier heights for
5 channels 1(a), 1(b) and 1(c). A reduction of the barrier heights of channels 1(a), 1(b) and 1(c)
6 of 2.5 kcal mol⁻¹ has been made, to give ΔE_e^\ddagger values of 1.72, 3.22 and 4.75 kcal mol⁻¹ for
7 these channels, and rate coefficient calculations were carried out with the corresponding HL
8 F12ave/CBSave IRC. This lowering of 2.5 kcal.mol⁻¹ in the ΔE_e^\ddagger values made for channels
9 1(a), 1(b) and 1(c) is similar to the downward correction we had to make in related studies of
10 the Cl + CH₃C(O)OCH₃ ⁴⁹ and Cl + HCOOH ⁵⁶ reactions of 2.2 and 2.7 kcal.mol⁻¹
11 respectively. k_{total} ICVT/SCT values obtained at different temperatures with this correction
12 are shown in column 2 of Table 8. As can be seen from this table, the experimental rate
13 coefficients fall into two groups. A lower set, where the experimental values of Talukdar ¹⁴
14 and Shallcross ¹⁵ show a positive temperature dependence in the temperature range 220-420
15 K, and a higher group, where the experimental values of Nielsen ¹⁸ show a negative
16 temperature dependence in the temperature range 298-393 K. At 300 K, the computed
17 $k^{\text{ICVT/SCT}}$ value with the HL F12ave/CBSave IRC is ~ 30 times lower than the 300 K values
18 of Talukdar ¹⁴ and Shallcross ¹⁵. However, a 2.5 kcal.mol⁻¹ reduction of the ΔE_e^\ddagger values for
19 channels 1(a), 1(b) and 1(c) increases the 300 K $k^{\text{ICVT/SCT}}$ value, to give good agreement with
20 the 300 K values of Talukdar ¹⁴ and Shallcross ¹⁵. These computed $k^{\text{ICVT/SCT}}$ values also
21 show a positive temperature dependence, as observed in the work of Talukdar and Shallcross
22 (see Figure 8). To increase the computed $k^{\text{ICVT/SCT}}$ 300 K value to agree with the higher
23 value of Nielsen ¹⁸, requires a reduction in barrier heights ΔE_e^\ddagger of at least 3.5 kcal.mol⁻¹.
24 With such a reduction a positive temperature dependence of $k^{\text{ICVT/SCT}}$ is still computed, not a
25 negative temperature dependence as observed by Nielsen ¹⁸. Also, a reduction of ΔE_e^\ddagger of 3.5
26 kcal.mol⁻¹ is larger than we have had to apply to calculations at the same level on related
27 reactions ^{49,56} to give acceptable agreement with experimental values. Therefore, considering
28 all the evidence it is concluded that the lower set of experimental rate coefficients, with a
29 positive temperature dependence, are to be preferred. As has been noted previously ^{49,56}, the
30 main reason for the difference between the experimental and computed rate coefficients is
31 because the equilibrium geometries and vibrational frequencies of the stationary points on the
32 reaction surface, and the entropy term used in the calculation of the rate coefficient come
33 from the lower level calculations (M06-2X/6-31+G** in this case) whereas the higher level
34 calculations give the enthalpy term used in the calculation of the rate coefficient. This is
35 discussed further in the Concluding Remarks.
36
37
38
39
40
41
42
43
44
45
46
47
48
49
50
51
52
53
54
55
56
57
58
59
60

Atmospheric Implications

Both the M06-2X/6-31+G** single level and UCCSD(T*)F12ave/CBSave//M06-2X/6-31+G** improved single level electronic structure / rate coefficient calculations performed in this work favour the lower set of experimental rate coefficients¹⁴⁻¹⁷ over the higher group^{18,19}. They also support the positive temperature dependence of the rate coefficient in the temperature range 200-400 K observed in the work of refs (14) and (15) rather than the negative temperature dependence observed in ref.(18).

It is valuable to compare the results of this present work on the OH + CH₃ONO₂ reaction with those obtained in our earlier work on the Cl + CH₃ONO₂ reaction¹¹. Both proceed via a hydrogen abstraction reaction. For the Cl + CH₃ONO₂ reaction, the recommended values for the reaction barrier (ΔE_e^\ddagger) and reaction enthalpy (ΔH_{298K}^{RX}) are 0.17 and -2.30 kcal.mol⁻¹, values obtained at the UCCSD(T*)-F12/CBS//M06-2X/6-31+G** level, whereas the corresponding recommended values in this work for the OH + CH₃ONO₂ case are 1.72 (1a) and -17.72 kcal.mol⁻¹. The reaction barrier (ΔE_e^\ddagger) is lower in the Cl + CH₃ONO₂ case than in the OH + CH₃ONO₂ reaction, and the Cl + CH₃ONO₂ rate coefficients are higher, in the temperature range 200-400 K. The Cl + CH₃ONO₂ reaction rate coefficient shows a positive temperature dependence as is now established for the OH + CH₃ONO₂ case. For the OH + CH₃ONO₂ reaction, as shown in Figure 1, TS_{1a} has a structure with a hydrogen bond between the O of the O-H and an H of the CH₃ group, and a longer hydrogen bond between the H of the O-H and an O of the -NO₂ group. In the Cl + CH₃ONO₂ case, this hydrogen bonding is obviously not possible and the transition state structure is similar to that shown for TS_{1b} and TS_{1c} in Figure 1.

As was noted in the Introduction, the lifetime of methyl nitrate in the troposphere is controlled by photolysis, reaction with Cl atoms and reaction with OH. The photolysis lifetime of methyl nitrate in the troposphere (0-15 km above ground level) has been determined to be in the region of 1-5 days^{1,12,13}. In the troposphere the temperature typically drops from 288 K at ground level to 216 K at 15 km, and hence the rate coefficients shown in Table 8 in the temperature range 200-300 K are the most relevant to the troposphere. In our earlier work on Cl + CH₃ONO₂¹¹, we calculated that for [Cl] = 10³ atom.cm⁻³, the estimated day-time global average in the marine boundary layer⁵⁷, the methyl nitrate lifetime with respect to this reaction is 3.68x10⁴ days at 300 K and 2.49x10⁵ days at 200 K, using the now well established Cl + CH₃ONO₂ rate coefficients¹¹. For the OH + CH₃ONO₂ reaction, the work of Talukdar et al.¹⁴ is the only study in which rate coefficients have been measured in

1
2
3 the range 200-300 K. The 298 K rate coefficient of ref.(14) is in the lower group. Also, the
4 rate coefficients determined by these authors in the higher temperature region 300-423 K
5 agree reasonably well with previously determined values in this temperature range by
6 Shallcross et al. ¹⁵. The experimental rate coefficients of Talukdar et al. ¹⁴ were therefore
7 assumed as a reliable reference for the purposes of calculating the lifetime of methyl nitrate
8 with respect to reaction with OH. This can be calculated at a particular temperature as $1/(k_{OH}$
9 $[OH])$, if $[OH]$ and k_{OH} , the $OH + CH_3ONO_2$ rate coefficient, are known at that
10 temperature. Using $[OH] = 1 \times 10^6 \text{ molecule.cm}^{-3}$, the estimated average day-time concentration
11 of OH ⁵⁸, with the rate coefficients from Talukdar et al. ¹⁴ (see Table 8), the methyl nitrate
12 lifetime with respect to reaction with OH is calculated as 422 (300K) and 2320 (200K) days
13 respectively. Therefore, under normal atmospheric conditions in the troposphere the methyl
14 nitrate lifetimes are in the order

$$\text{Photolysis} < OH_{\text{reaction}} < Cl_{\text{reaction}}$$

28 Concluding remarks

29
30 The reaction mechanism of the $OH + CH_3ONO_3$ reaction has been investigated by
31 carrying out *ab initio*/DFT calculations on four possible reaction channels:- hydrogen atom
32 abstraction, NO_2 production, NO_3 production and HNO_3 production. All reaction channels are
33 exothermic but the H abstraction channel has a much lower activation energy compared with
34 the other channels. This means that the H abstraction channel will have the highest rate
35 coefficients and is therefore kinetically the most important while NO_2 , NO_3 and HNO_3
36 formation will be minor. The H abstraction channel was found to proceed via three possible
37 pathways involving transition states TS_{1a} , TS_{1b} and TS_{1c} (see Figure 1-3). The pathway via
38 TS_{1a} , a hydrogen bonded transition state, has the lowest activation energy.

39
40
41
42
43
44
45
46
47
48
49
50
51
52
53
54
55
56
57
58
59
60
ICVT/SCT rate coefficients obtained with the UCCSD(T*)-F12ave/CBSave//M06-2X
IRC for the H abstraction reaction (reaction 1) via the three transition states, TS_{1a} , TS_{1b} and
 TS_{1c} , show that k_{1a} and k_{1b} are the main contributors to the overall rate coefficient ($k_{\text{total}} = 2k_{1a}$
 $+ 2k_{1b} + k_{1c}$) in the temperature range 200-400 K. k_{1c} makes a negligible contribution. k_{1a} is
greater than k_{1b} in the atmospherically important temperature range 200-300K in the
troposphere with k_{1b} becoming greater than k_{1c} at $T > 334$ K. A reduction in the barrier
heights (ΔE_e^\ddagger) of TS_{1a} , TS_{1b} and TS_{1c} by $2.5 \text{ kcal.mol}^{-1}$ brings the computed k_{total} values in
reasonably good agreement with the experimental values over the range 200-400 K. k_{1a} , k_{1b}
and k_{1c} all increase with increasing temperature. This behaviour as well as the fact that the

k_{total} is less than the lower group of experimental rate coefficients favours the lower experimental rate coefficients over the higher group. The relative importance of the methyl nitrate loss processes (photolysis, reaction with OH and reaction with Cl atoms) in the troposphere is discussed and the methyl nitrate lifetimes with respect to these processes is shown to be in the order

$$\text{Photolysis} < \text{OH}_{\text{reaction}} < \text{Cl}_{\text{reaction}} .$$

In summary, the rate coefficients computed at the highest level favour the lower set of experimental rate coefficients, which show a positive temperature dependence. However, the computed lower level (M06-2X/6-31+G**) rate coefficients agree better with these experimental values than the rate coefficients computed at the higher level (UCCSD(T*)F12ave/CBSave//M06-2X/6-31+G**). This type of discrepancy has been noted before⁵⁹. At present, with wavefunction methods, one can carry out systematic improvements in the computation of relative electronic barriers, with the geometries of the reactants, RC, TS, PC and products obtained at a lower level (M06-2X/6-31+G** in this case). In this connection, there is little more that we can do to improve the enthalpy of activation as UCCSD(T*)-F12-CBS is at present at the state-of-the-art level. (It should also be noted that it is inappropriate to compare computed activation energies with experimentally derived activation energies; see our previous work^{11,49,56}). Regarding geometrical structures and vibrational frequencies, a method with analytical first and second derivatives is required. We have previously shown that using different functionals for the lower level, for geometries and frequencies, with the same higher level barrier height can lead to computed rate coefficients which differ by one order of magnitude as the entropic contribution to the free energy of activation will be different with different functionals^{11,49,56}. In summary, one should bear in mind that the uncertainties associated with the entropic and/or enthalpic contributions can lead to computed uncertainties in the computed rate coefficients. Further theoretical and experimental investigations are required to bring theory closer to experiment for this reaction, with the evidence from the present work clearly favouring the lower set of experimental rate coefficients.

Contents of Supporting Information

SI1. A note on calculation of improved single-level V_{MEP} curves

SI12 Extra information on NO₂ formation:



SI3 Extra information on NO₃ formation:



5 **SI4** Extra information on HNO₃ formation:
6



9 **SI5.** Table SI1. $k^{\text{ICVT/SCT}}$ values obtained with the HL UCCSD(T*)-F12ave/CBSave//M06-2X
10 IRC for $2k_{1a}$, $2k_{1b}$ and k_{1c} from barrier heights (ΔE_e^\ddagger) of 4.22, 5.72 and 7.25 kcal mol⁻¹
11 respectively.

12 **SI6.** Table SI2. $k^{\text{ICVT/SCT}}$ values obtained with the HL UCCSD(T*)-F12ave/CBSave//M06-2X
13 IRC for $2k_{1a}$, $2k_{1b}$ and k_{1c} from barrier heights (ΔE_e^\ddagger) of 1.72, 3.22 and 4.75 kcal mol⁻¹
14 respectively. ΔE_e^\ddagger values for 1a, 1b and 1c are reduced by 2.5 kcal.mol⁻¹ from those used in
15 SI5 (see text).
16
17
18
19
20
21
22
23
24

25 **Acknowledgements**

26
27 The authors are grateful to the Research Grant Council (RGC) of the Hong Kong
28 Special Administrative Region (HKSAR, Grant Numbers: PolyU 5018/13P and 153013/15P),
29 the Research Committee of the Hong Kong Polytechnic University (Account No. A-PK41
30 and G-YG99) and NERC (UK) for support, and the National Service for Computational
31 and G-YG99) and NERC (UK) for support, and the National Service for Computational
32 Chemistry Software (NSCCS), EPSRC (UK) for computational resources.
33
34
35
36
37
38
39
40
41
42
43
44
45
46
47
48
49
50
51
52
53
54
55
56
57
58
59
60

References

1. Roberts, J. M. The Atmospheric Chemistry of Organic Nitrates *Atmos. Environ. Part A-General Topics* **1990**, *24*, 243-287.
2. Clemitshaw, K. C.; Williams, J.; Rattigan, O. V.; Shallcross, D. E.; Law, K. S.; Cox, R. A. Gas-phase Ultraviolet Absorption Cross-sections and Atmospheric Lifetimes of C2-C6 Alkyl Nitrates *J Photochem Photobiol A* **1997**, *102*, 117-126.
3. Ballschmiter, K. Atmospheric Chemistry: A Marine Source for Alkyl Nitrates *Science* **2002**, *297*, 1127-1128.
4. Atlas, E.; Pollock, W.; Greenberg, J.; Heidt, L.; Thompson A. M. Alkyl Nitrates, Non-Methane Hydrocarbons and Halocarbon Gases over the Equatorial Pacific-Ocean during SAGA3 *J. Geophys. Res.-Atmos.* **1993**, *98*, 16933-16947.
5. Blake, N. J.; Blake, D. R.; Swanson, A. L.; Atlas, E.; Flocke, F.; Rowland, F. S. Latitudinal, Vertical and Seasonal Variations of C1-C4 Alkyl Nitrates in the Troposphere over the Pacific Ocean during PEM-Tropics A and B: Ocean and Continental Sources *J. Geophys. Res. Atmos.* **2003**, *108*, 8242, Issue D2.
6. Chuck, A. L.; Turner, S. M.; Liss, P. S. Direct Evidence for a Marine Source of C-1 and C-2 Alkyl Nitrates *Science* **2002**, *297*, 1151-1154.
7. Darnall, K. R.; Carter, W. P. L.; Winer, A. M.; Lloyd, A. C.; Pitts, J. N. Importance of RO₂ + NO in Alkyl Nitrate Formation from C4-C6 Alkane Photooxidation under Simulated Atmospheric Conditions *J. Phys. Chem.* **1976**, *80*, 1948-1950.
8. He, S.; Chen, Z.; Zhang, X. Photochemical Reactions of Methyl and Ethyl Nitrate: A Dual Role for Alkyl Nitrates in the Nitrogen Cycle *Environ. Chem.*, **2011**, *8*, 529-542
9. Wu, S.; Mickley, J.L.; Jacob, D.J.; Logan, J.A.; Yantosca, R.M.; Rind, D. Why are there Large Differences between Models in Global Budgets of Tropospheric Ozone? *J. Geophys Res* **2007**, *112*, D05302, Issue D5
10. Horowitz, L.W.; Fiore, A.M.; Milly, G.P.; Cohen, R.C.; Perring, A.; Wooldridge, P.J.; Hess, P.G.; Emmons, L.K.; Lamarque, J.F. Observational Constraints on the Chemistry of Isoprene Nitrates over the Eastern United States *J. Geophys Res* **2007**, *112*, D12S08, Issue D12
11. Ng, M.; Mok, D.K.W.; Lee, E.P.F.; Dyke, J.M. A Theoretical Study of the Mechanism of the Atmospherically Relevant Reaction of Chlorine Atoms with Methyl Nitrate, and Calculation of the Reaction Rate Coefficient at Temperatures Relevant to the Troposphere *Phys Chem Chem Phys* **2015**, *17*, 7463-7476
12. Talukdar, R.K.; Burkholder, J.B.; Hunter, M.; Gilles, M.K.; Roberts, J.M.; Ravishankara, A.V. Atmospheric Fate of Several Alkyl Nitrates 1. Rate Coefficients of the Reactions of Alkyl Nitrates with Isotopically Labelled Hydroxyl Radicals *J. Chem Soc Faraday* **1997**, *93*, 2797-2805
13. Taylor, W.D.; Allston, T.D.; Moscato, M.J.; Fazekas, G.B.; Kozlowski, R.; Takacs, G.A. Atmospheric Photo-dissociation Lifetimes for Nitromethane, Methyl Nitrite and Methyl Nitrate *Int J. Chem. Kinetic.* **1980**, *12*, 231-240
14. Talukdar, R. K.; Herndon, S. C.; Burkholder, J. B.; Roberts, J. M.; Ravishankara, A. R. Atmospheric Fate of Several Alkyl Nitrates 2. UV Absorption Cross-sections and Photodissociation Quantum Yields *J. Chem. Soc. Faraday Trans:* **1997**, *93*, 2787-2796.
15. Shallcross, D. E.; Biggs, P.; CanosaMas, C. E.; Clemitshaw, K. C.; Harrison, M. G.; Alanon, M. R. L.; Pyle, J. A.; Vipond, A.; Wayne, R. P. Rate Constants for the Reaction between OH and CH₃ONO₂, and C₂H₅ONO₂ over a range of Pressure and Temperature *J. Chem. Soc. Faraday Trans* **1997**, *93*, 2807-2811.
16. Gaffney, J. S.; Fajer, R.; Senum, G. I.; Lee, J. H. Measurement of the Reactivity of OH with Methyl Nitrate--Implications for Prediction of Alkyl Nitrate-OH Reaction Rates

1
2
3
4
5
6
7
8
9
10
11
12
13
14
15
16
17
18
19
20
21
22
23
24
25
26
27
28
29
30
31
32
33
34
35
36
37
38
39
40
41
42
43
44
45
46
47
48
49
50
51
52
53
54
55
56
57
58
59
60

Int.J.Chem.Kinetic. **1986**, *18*, 399-407.

17. Kakesu, M.; Bandow, H.; Takenaka, N.; Maeda, Y.; Washida, N. Kinetic Measurements of Methyl and Ethyl Nitrate Reactions with OH Radicals *Int.J.Chem. Kinetic.* **1997**, *29*, 933-941.

18. Nielsen, O. J.; Sidebottom, H. W.; Donlon, M.; Treacy, J. An Absolute-rate and Relative-Rate Study of the Gas-phase Reaction of OH Radicals and Cl Atoms with Normal Alkyl Nitrates *Chem. Phys. Letts* **1991**, *178*, 163-170.

19. Kerr, J. A.; Stocker, D. W. Kinetics of the Reactions of Hydroxyl Radicals with Alkyl Nitrates and with some Oxygen-containing Organic-compunds Studied under Simulated Atmospheric Conditions *J.Atmos. Chem.* **1986**, *4*, 253-262.

20. Cox, A.P.; Waring, S. Microwave Spectrum, Structure and Dipole Moment of Methyl Nitrate *Trans Far Soc* **1971**, *67*, 3441-3449

21. Zhao, Y.; Truhlar, D. G. The M06 Suite of Density Functionals for Main Group Thermochemistry, Thermochemical Kinetics, Noncovalent Interactions, Excited States, and Transition Elements: Two New Functionals and Systematic Testing of Four M06-class Functionals and 12 other Functionals *Theor. Chem. Acc.* **2008**, *120*, 215-241.

22. Frisch, M. J.; Trucks, G. W.; Schlegel, H. B.; Scuseria, G. E.; Robb, M. A.; Cheeseman, J. R.; Scalmani, G.; Barone, V.; Mennucci, B.; Petersson, G. A. et al Gaussian 09; Revision B.01 ed.; Gaussian, Inc.: Wallingford CT, 2010.

23. Goerigk, L.; Grimme, S. A Thorough Benchmark of Density Functional Methods for General Main Group Thermochemistry, Kinetics and Non-covalent Interactions *Phys Chem Chem Phys* **2011**, *13*, 6670-6688.

24. Zheng, J. J.; Zhao, Y.; Truhlar, D. G. The DBH24/08 Database and its Use to Assess Electronic Structure Model Chemistries for Chemical Reaction Barrier Heights *J Chem. Theory Comput.* **2009**, *5*, 808--821.

25. Zhao, Y.; Truhlar, D. G. Density Functionals with Broad Applicability in Chemistry *Acc.Chem. Res.* **2008**, *41*, 157-167.

26. Xu, X. F.; Alecu, I. M.; Truhlar D. G. How Well can Modern Density Functionals Predict Internuclear Distances at Transition States? *J Chem.Theory Comput.* **2011**, *7*, 1667-1676.

27. Hratchian, H. P.; Schlegel, H. B. Accurate Reaction Paths using a Hessian Predictor-Corrector Integrator *J.Chem.Phys.* **2004**, *120*, 9918-9924.

28. Hratchian, H. P.; Schlegel, H. B. Finding Minima, Transition States, and Following Reaction Pathways on ab initio Potential Energy Surfaces. In *Theory and Applications of Computational Chemistry: The First Forty Years*; Dykstra, C. E.; Frenking, G.; Kim, K. S.; Scuseria, G. E.; Eds.; Elsevier: Amsterdam, **2005**; pp 195-249.

29. Hratchian, H. P.; Schlegel H. B. Using Hessian Up-dating to Increase the Efficiency of a Hessian based Predictor-Corrector Reaction Path Following Method *J.Chem.Theory Comput.* **2005**, *1*, 61-69.

30. Knizia, G.; Adler, T. B.; Werner, H. J. Simplified CCSD(T)-F12 Methods: Theory and Benchmarks *J.Chem. Phys.* **2009**, *130*, 054104.

31. Werner, H. J.; Knizia, G; Manby, F. R. Explicitly Correlated Coupled Cluster Methods with Pair-specific Geminals *Mol Phys* **2011**, *109*, 407-417.

32. Werner, H.-J.; Knowles, P. J.; Knizia, G.; Manby, F. R.; Schütz, M.; Celani, P.; Korona, T.; Lindh, R.; Mitrushenkov, A.; Rauhut, G. et al. MOLPRO, version 2012.1, A Package of ab initio programs.

33. Werner, H. J.; Knowles, P. J.; Knizia, G.; Manby, F. R.; Schutz, M. MOLPRO: A General Purpose Quantum Chemistry Program Package *Wiley Interdisciplinary Reviews- Comput Mol Sci* **2012**, *2*, 242-253.

34. Peterson, K. A.; Adler, T. B.; Werner, H. J. Systematically Convergent Basis Sets For Explicitly Correlated Wavefunctions: The Atoms H, He, B-Ne and Al-Ar *J.Chem.Phys.* **2008**,

1
2
3 128, 084102.

4 35. Weigend, F.; Kohn, A.; Hattig, C. Efficient Use of the Correlation Consistent Basis Sets in
5 Resolution of the Identity MP2 Calculations *J. Chem. Phys.* **2002**, *116*, 3175-3183.

6 36. Helgaker, T.; Klopper, W.; Koch, H.; Noga, J. Basis-set Convergence of Correlated
7 Calculations on Water *J. Chem. Phys.* **1997**, *106*, 9639-9646.

8 37. Halkier, A.; Helgaker, T.; Klopper, W.; Jorgensen, P.; and Csaszar, A. G. Comment on
9 "Geometry Optimization with an Infinite Basis set" (*J. Phys. Chem. A*, **1999**, *103*, 651) and
10 "Basis Set Extrapolation" (*Chem. Phys. Letts* **1988**, *294*, 45) *Chem. Phys. Letts* **1999**, *310*,
11 385-389.

12 38. Schwenke, D. W. The Extrapolation of One-electron Basis Sets in Electronic Structure
13 Calculations. How It Should Work and How It Can Be Made to Work. *J. Chem. Phys.* **2005**,
14 *122*, 014107.

15 39. Hill, J. G.; Peterson, K. A.; Knizia, G.; Werner, H. J. Extrapolating MP2 and CCSD
16 Explicitly Correlated Energies to the Complete Basis Set Limit with First and Second Row
17 Correlation Consistent Basis Sets *J. Chem. Phys.* **2009**, *131*, 194105.

18 40. Li, G. X.; Gao, T.; Chen, D.; Li, Y. X.; Zhang, Y. G.; Zhu, Z. H. The Splitting of Low-lying
19 States for the Hydroxyl Molecule under Spin-orbit Splitting *Chinese Phys.* **2006**, *15*, 998-
20 1003.

21 41. Zheng, J.; Zhang, S.; Lynch, B. J.; Corchado, J. C.; Chuang, Y.-Y.; Fast, P. L.; Hu, W.-P.;
22 Liu, Y.-P.; Lynch, G. C.; Nguyen, K. A. et al. POLYRATE 2010-A; 2010 ed.; Department of
23 Chemistry and Supercomputing Institute, University of Minnesota: Minneapolis, Minnesota,
24 **2010**.

25 42. Truhlar, D. G. A Simple Approximation for the Vibrational Partition-function of a
26 Hindered Internal-Rotation *J. Comput. Chem.* **1991**, *12*, 266-270.

27 43. Chuang, Y. Y.; Truhlar, D. G. Statistical Thermodynamics of Bond Torsional Modes
28 *J. Chem. Phys.* **2000**, *112*, 1221-1228.

29 44. Ellingson, B. A.; Lynch, V. A.; Mielke, S. L.; Truhlar, D. G. Statistical Thermodynamics of
30 Bond Torsional Modes: Tests of Separable, Almost Separable and Improved Pitzer-Gwinn
31 Approximations *J. Chem. Phys.* **2006**, *125*, 084305.

32 45. Garrett, B. C.; Redmon, M. J.; Steckler, R.; Truhlar, D. G.; Baldrige, K. K.; Bartol, D.;
33 Schmidt, M. W.; Gordon, M. S. Algorithms and Accuracy Requirements for Computing
34 Reaction Paths by the Method of Steepest Descent *J. Phys. Chem.* **1988**, *92*, 1476-1488.

35 46. Nguyen, K. A.; Jackels, C. F.; Truhlar, D. G. Reaction-path Dynamics in Curvilinear
36 Internal Coordinates including Torsions *J. Chem. Phys.* **1996**, *104*, 6491-6496.

37 47. Chuang, Y. Y.; Truhlar, D. G. Reaction Path Dynamics in Redundant Internal Coordinates
38 *J. Phys. Chem. A* **1998**, *102*, 242-247.

39 48. Chuang, Y. Y.; Corchado, J. C.; Truhlar, D. G. Mapped Interpolation Scheme for Single-
40 point Energy Corrections in Reaction Path Calculations and a Critical Evaluation of Dual-
41 level Reaction Path Dynamics Methods *J. Phys. Chem. A* **1999**, *103*, 1140-1149.

42 49. Chow, R.; Ng, M.; Mok, D. K. W.; Lee, E. P. F.; Dyke, J. M. Rate coefficients of the $\text{Cl} + \text{CH}_3\text{C}(\text{O})\text{OCH}_3 \rightarrow \text{HCl} + \text{CH}_3\text{C}(\text{O})\text{OCH}_2$ Reaction at Different Temperatures calculated
43 by Transition-state Theory with ab initio and Density Functional Theory Reaction Paths
44 *J. Phys. Chem. A* **2014**, *118*, 2040-2055.

45 50. Burcat, A.; Ruscic, B. Third Millennium Ideal Gas and Condensed Phase Thermochemical
46 Database for Combustion with updates from Active Thermochemical Tables; Aerospace
47 Engineering, and Argonne National Laboratory, Chemistry Division, **2005**; Vol. ANL-05/20
48 and TAE 960 Technion-IIT.

49 51. Ruscic, B.; Pinzon, R. E.; Morton, M. L.; Srinivasan, N. K.; Su, M. C.; Sutherland, J. W.;
50 Michael, J. V. Active Thermochemical Tables: Accurate Enthalpy of Formation of the
51 Hydroperoxy Radical HO_2 *J. Phys. Chem. A* **2006**, *110*, 6592-6601.
52
53
54
55
56
57
58
59
60

- 1
2
3 52. Cox, J. D.; Wagman, D. D.; Medvedev V. A. *CODATA Key Values for Thermodynamics*;
4 Hemisphere: New York, **1984**.
- 5
6 53. Garrett, B. C.; Truhlar, D. G.; Grev, R. S.; Magnuson A. W. Improved Treatment of
7 Threshold Contributions in Variational Transition-state Theory *J.Phys.Chem.* **1980**, *84*, 1730-
8 1748.
- 9
10 54. Fernandez-Ramos, A.; Ellingson, B. A.; Garrett, B. C.; Truhlar, D. G. Variational
11 Transition State Theory with Multidimensional Tunneling. In *Reviews in Computational*
12 *Chemistry*; Lipkowitz K. B., Cundari T. R., Eds.; Wiley-VCH: Hoboken, NJ, **2007**; Vol. 23;
13 pp 125.
- 14
15 55. Garrett, B. C.; Truhlar, D. G. Generalised Transition State Theory Calculations for the
16 Reactions D + H₂ and H + D₂ using an Accurate Potential energy Surface: Explanation of the
17 Kinetic Isotope Effect *J. Chem. Phys.* **1980**, *72*, 3460-3471.
- 18
19 56. Ng, M.; Mok, D.K.W.; Lee, E.P.F.; Dyke, J.M. A Theoretical Investigation of the
20 Atmospherically Important Reaction between Chlorine Atoms and Formic acid:
21 Determination of the Reaction Mechanism and Calculation of the Rate Coefficient at
22 Different Temperatures
23 *Mol.Phys.* **2015**, *113*, 1511-1533
- 24
25 57. Young, C.J.; Washenfelder, R.A.; Edwards, P.M.; Parrish, D.D.; Gilman, J.B.; Kuster,
26 W.C.; Mielke, L.H.; Osthoff, H.D.; Tsai, C.; Pikelnaya, O. et al. Chlorine as a Primary
27 Radical: Evaluation of Methods to Understand its Role in Initiation of Oxidative Cycles
28 *Atmos. Chem. Phys.*, **2014**, *14*, 3427-3440.
- 29
30 58. Finlayson-Pitts, B.J.; Pitts J.N. Jr., *Chemistry of the Upper and Lower Atmosphere*
31 (Academic Press, San Diego, **2000**)
- 32
33 59. Zheng, J.; Truhlar, D.G. Multi-path Variational Transition State Theory for Chemical
34 Reaction Rates of Complex Polyatomic Species: Ethanol + OH *Faraday Discussions* **2012**,
35 *157*, 59-88
- 36
37 60. Khursan, S. L.; Martem'yanov, V. S. Thermochemistry of Peroxy Radical Recombination
38 *Russ.J.Phys. Chem.* **1991**, *65*, 321-330.
- 39
40 61. Sander, S. P.; Abbatt, J.; Barker, J. R.; Burkholder, J. B.; Friedl, R. R.; Golden, D. M.;
41 Huie, R. E.; Kolb, C. E.; Kurylo, M. J.; Moortgat, G. K. et al. Chemical Kinetics and
42 Photochemical Data for Use in Atmospheric Studies; JPL Publication 10-6, Jet Propulsion
43 Laboratory: Pasadena, **2011**; Vol. Evaluation No. 17.
- 44
45 62. Hine, J.; Arata, K. *B Keto-enol Tautomerism 2. Calorimetric Determination of*
46 *Equilibrium Constants for Keto-enol Tautomerism of Cyclohexane and Acetone* *Chem Soc*
47 *Jpn* **1976**, *49*, 3089-3092.
- 48
49 63. Baroody, E. E.; Carpenter, G. A. Heats of Formation of Propellant Compounds; Rpt.
50 Naval Ordnance Systems Command Task No. 331-003/067-1/UR2402-001 for Naval
51 Ordnance Station, Indian Head, MD, **1972**; pp 1.
- 52
53 64. Chao, J.; Rossini, F. D. Heats of Combustion, Formation and Isomerization of Nineteen
54 Alkanols *J.Chem.Eng. Data* **1965**, *10*, 374-379.
- 55
56 65. Green, J. H. S. Revision of the Values of the Heats of Formation of Normal Alcohols
57 *Chemistry and Industry* **1960**, 1215-1216.
- 58
59 66. Parks, G. S. Thermal Data on Organic Compounds I. The Heat Capacities and Free
60 Energies of Methyl, Ethyl and Normal-butyl Alcohols *J.Am. Chem.Soc.* **1925**, *47*, 338-345.
- 61
62 67. Richards, T. W.; Davis H. S. The Heats of Combustion of Benzene, Toluene, Aliphatic
63 Alcohols, Cyclohexanol and other Carbon Compounds *J. Am.Chem. Soc.* **1920**, *42*, 1599-
64 1617.
- 65
66 68. Chase, M. W. Jr. NIST-JANAF Thermochemical Tables 4th Edition, Monograph 9 (Parts I
67 and II) *J.Phys.Chem.Ref.Data* **1998**, *27*, issue 6, 1-2.
- 68
69. Huber, K. P.; Herzberg, G. *Molecular Spectra and Molecular Structure IV Constants of*

1
2
3 Diatomic Molecules. **1979** Van Nostrand Reinhold , New York

4 70. Tsang, W. Heats of Formation of Organic Free Radicals by Kinetic Methods. In *Energetics*
5 *of Organic Free Radical*; Martinho Simoes, J. A., Greenberg, A., Liebman, J. F., Eds.;

6 Blackie Academic and Professional: London, **1996**, 22-58.

7 71. Wadso, I. Heats of Vaporization for a Number of Organic Compounds

8 *Acta Chem.Scand.* **1966**, 20, 544-532
9
10
11
12
13
14
15
16
17
18
19
20
21
22
23
24
25
26
27
28
29
30
31
32
33
34
35
36
37
38
39
40
41
42
43
44
45
46
47
48
49
50
51
52
53
54
55
56
57
58
59
60

Table 1. Computed reaction (ΔE_e^{RX}) and activation (ΔE_e^\ddagger) energies (in kcal mol⁻¹) of the OH + CH₃ONO₂ → TS₂ → CH₃OOH + NO₂ channel at various UCCSD(T*)-F12x//M06-2X/6-31+G** levels of calculation.

Methods	ΔE_e^{RX}			ΔE_e^\ddagger		
	F12a	F12b	(other)	F12a	F12b	(other)
(M06-2X/6-31+G**)			(0.28)			(29.86)
UCCSD(T*)-F12x/VTZ-F12	-1.81	-1.75		23.38	23.56	
UCCSD(T*)-F12x/VQZ-F12	-1.76	-1.72		23.82	23.90	
1/X ³ CBS1	-1.72	-1.71		24.14	24.15	
Schwenke CBS2	-1.74	-1.72		23.98	24.03	
Average ΔE_e (CBS1 and CBS2)	-1.73	-1.71		24.06	24.09	
Best ΔE_e (F12ave/CBSave) ^a			-1.72(1)			24.08(17)
ΔE_{0K} (CBSave)	-1.42	-1.40		24.35	24.38	
ΔE_{0K} (include SO of OH)	-1.22	-1.20		24.55	24.58	
Best ΔE_{0K} (F12ave/CBSave) ^a			-1.21			24.56
ΔH_{298K}	-1.36	-1.35				
ΔH_{298K} (including SO of OH)	-1.16	-1.15				
Best ΔH_{298K} (F12ave/CBSave) ^a			-1.16			
ΔH_{298K} (from available $\Delta H_{f,298K}$)			-2.96 ^b -2.41 ^c			

^a The average of four CBS values (uncertainties w.r.t. F12b/VQZ-F12 values).

^b Using $\Delta H_{f,298K}$ values of CH₃ONO₂, -29.16 kcal mol⁻¹;⁵⁰ OH, 8.93 kcal mol⁻¹;⁵¹ CH₃OOH, -31.31 kcal mol⁻¹;⁶⁰ NO₂, 8.12 kcal mol⁻¹.^{51,61}

^c Using the $\Delta H_{f,298K}$ value of -29.71 kcal mol⁻¹, which was computed in our previous study,¹¹ for CH₃ONO₂ instead of the value from Burcat⁵⁰ given in footnote (b).

Table 2. Computed reaction (ΔE_e^{RX}) and activation (ΔE_e^\ddagger) energies (in kcal mol⁻¹) of the OH + CH₃ONO₂ → TS₃ → CH₃OH + NO₃ channel at various UCCSD(T*)-F12x//M06-2X/6-31+G** levels of calculation.

Methods	ΔE_e^{RX}			ΔE_e^\ddagger		
	F12a	F12b	(other)	F12a	F12b	(other)
(M06-2X/6-31+G**)			(-2.21)			(37.71)
UCCSD(T*)-F12x/VTZ-F12	-8.31	-8.33		35.64	35.76	
UCCSD(T*)-F12x/VQZ-F12	-8.11	-8.11		35.91	35.97	
1/X ³ CBS1	-7.96	-7.95		36.11	36.12	
Schwenke CBS2	-8.03	-8.03		36.01	36.04	
Average ΔE_e (CBS1 and CBS2)	-7.99	-7.99		36.06	36.08	
Best ΔE_e (F12ave/CBSave) ^a			-7.99(12)			36.07(11)
ΔE_{0K} (CBSave)	-7.93	-7.93		36.88	36.90	
ΔE_{0K} (include SO of OH)	-7.73	-7.73		37.08	37.10	
Best ΔE_{0K} (F12ave/CBSave) ^a			-7.73			37.09
ΔH_{298K}	-8.21	-8.21				
ΔH_{298K} (including SO of OH)	-8.01	-8.01				
Best ΔH_{298K} (F12ave/CBSave) ^a			-8.01			
ΔH_{298K} (from available $\Delta H_{f,298K}$)			-11.77 ^b -11.22 ^c -9.83 ^{c,d}			

^a The average of four CBS values (uncertainties w.r.t. F12b/VQZ-F12 values).

^b Using $\Delta H_{f,298K}$ values of CH₃ONO₂, -29.16 kcal mol⁻¹,⁵⁰ OH, 8.93 kcal mol⁻¹,⁵¹ CH₃OH, -49.0 kcal mol⁻¹ (average of nine values);⁶²⁻⁶⁷ NO₃, 17.0 kcal mol⁻¹.⁶⁸

^c Using the $\Delta H_{f,298K}$ value of -29.71 kcal mol⁻¹, which was computed in our previous study,¹¹ for CH₃ONO₂ instead of the value from Burcat⁵⁰ given in footnote (b).

^d Using the $\Delta H_{f,298K}$ value of -47.61 kcal mol⁻¹, which was computed in the present study, for CH₃OH instead of the average of nine values given in footnote (b).

Table 3. Computed reaction energies (ΔE_e^{RX} ; in kcal mol⁻¹) obtained at different levels of calculation for the CH₃OH → CO + 2H₂ reaction, and the derived $\Delta H_{f,298K}$ value for CH₃OH.

ΔE_e^{RX}	UCCSD(T*)-F12a	UCCSD(T*)-F12b
VTZ-F12	34.11	34.03
VQZ-F12	34.40	34.36
1/X ³ CBS1	34.61	34.60
Schwenke CBS2	34.50	34.48
Best estimate (F12ave/CBSave) ^a		34.55
ΔE_{0K}^{RX} ($\Delta ZPE = -16.90$ kcal mol ⁻¹)		17.65
ΔH_{298K}^{RXb}		21.20
$\Delta H_{f,298K}(CH_3OH)^c$		-47.61
Experimental $\Delta H_{f,298K}(CH_3OH)$	-48.0, ^d -47.94, ^e -48.1 ± 1.2, ^f -48.21, ^g -48.33 ± 0.05, ^h -48.07 ± 0.05, ⁱ -50.86, ^j -50.98 ± 0.48, ^k -51.1 ± 1.2 ^l	

^a The average of the four UCCSD(T*)-F12x/CBS values.

^b $\Delta ZPE + \Delta E_v^{298K} + 6.5RT = -13.35$ kcal mol⁻¹.

^c Using $\Delta H_{f,298K}(CO) = -26.417 \pm 0.041$ kcal mol⁻¹ and the computed best F12ave/CBSave ΔH_{298K}^{RX} of 21.20 kcal mol⁻¹.

^d From Ref. [62].

^e Value computed using $\Delta H_{f,liquid}^\circ$ of -238.4 kJ mol⁻¹ from Ref. [63] and ΔH_{vap}° of 37.8 kJ mol⁻¹ from Ref. [65].

^f Value computed using $\Delta H_{f,liquid}^\circ$ of -238.4 kJ mol⁻¹ from Ref. [63] and ΔH_{vap}° of 8.91 kcal mol⁻¹ from Ref. [71].

^g Value computed using $\Delta H_{f,liquid}^\circ$ of -239.5 ± 0.2 kJ mol⁻¹ from Ref. [64] and ΔH_{vap}° of 37.8 kJ mol⁻¹ from Ref. [65].

^h Value computed using $\Delta H_{f,liquid}^\circ$ of -238.4 kJ mol⁻¹ from Ref. [64] and ΔH_{vap}° of 8.91 kcal mol⁻¹ from Ref. [71].

ⁱ From Ref. [65].

^j Value computed using $\Delta H_{f,liquid}^\circ$ of -250.6 kJ mol⁻¹ from Ref. [66] and ΔH_{vap}° of 37.8 kJ mol⁻¹ from Ref. [65].

^k Value computed using $\Delta H_{f,liquid}^\circ$ of -250.6 kJ mol⁻¹ from Ref. [66] and ΔH_{vap}° of 8.91 kcal mol⁻¹ from Ref. [71].

^l Value computed using $\Delta H_{f,liquid}^\circ$ from Ref. [67] and ΔH_{vap}° of 8.91 kcal mol⁻¹ from Ref.

[71].

1
2
3
4
5
6
7
8
9
10
11
12
13
14
15
16
17
18
19
20
21
22
23
24
25
26
27
28
29
30
31
32
33
34
35
36
37
38
39
40
41
42
43
44
45
46
47
48
49
50
51
52
53
54
55
56
57
58
59
60

Table 4. Computed reaction (ΔE_e^{RX}) and activation (ΔE_e^\ddagger) energies (in kcal mol⁻¹) of the OH + CH₃ONO₂ → TS_{4a} → CH₃O + HNO₃ channel at various UCCSD(T*)-F12x//M06-2X/6-31+G** levels of calculation.

Methods	ΔE_e^{RX}			ΔE_e^\ddagger		
	F12a	F12b	(other)	F12a	F12b	(other)
(M06-2X/6-31+G**)			(-7.32)			(31.88)
UCCSD(T*)-F12x/VTZ-F12	-6.47	-6.51		26.48	26.63	
UCCSD(T*)-F12x/VQZ-F12	-6.54	-6.56		27.01	27.06	
1/X ³ CBS1	-6.60	-6.59		27.39	27.37	
Schwenke CBS2	-6.57	-6.57		27.20	27.21	
Average ΔE_e (CBS1 and CBS2)	-6.58	-6.58		27.29	27.29	
Best ΔE_e (F12ave/CBSave) ^a			-6.58(3)			27.29(17)
ΔE_{0K} (CBSave)	-6.53	-6.53		28.62	28.62	
ΔE_{0K} (include SO of OH)	-6.33	-6.33		28.82	28.82	
Best ΔE_{0K} (F12ave/CBSave) ^a			-6.33			28.82
ΔH_{298K}	-6.98	-6.98				
ΔH_{298K} (including SO of OH)	-6.78	-6.78				
Best ΔH_{298K} (F12ave/CBSave) ^a			-6.78			
ΔH_{298K} (from available $\Delta H_{f,298K}$)			-7.77 ^b			
			-7.22 ^c			

^a The average of four CBS values (uncertainties w.r.t. F12b/VQZ-F12 values).

^b Using $\Delta H_{f,298K}$ values of CH₃ONO₂, -29.16 kcal mol⁻¹;⁵⁰ OH, 8.93 kcal mol⁻¹;⁵¹ CH₃O, 4.1 kcal mol⁻¹;⁷⁰ HNO₃, -32.101 kcal mol⁻¹.⁶⁸

^c Using the $\Delta H_{f,298K}$ value of -29.71 kcal mol⁻¹, which was computed in our previous study,¹¹ for CH₃ONO₂ instead of the value from Burcat⁵⁰ given in footnote (b).

Table 5. Computed ΔE_e , ΔE_{0K} and ΔH_{298K} (w.r.t. separate reactants; in kcal mol⁻¹) of various species in the OH + CH₃ONO₂ → TS_{4b} → CH₃O(OH)NO₂ conformer 1 → TS_{rot} → CH₃O(OH)NO₂ conformer 2 → TS_{4c} → CH₃O + HNO₃ channel obtained at various UCCSD(T*)-F12x//M06-2X/6-31+G** levels of calculation.

ΔE_e (in kcal mol ⁻¹)	TS _{4b}	CH ₃ O(OH)NO ₂ conformer 1	TS _{rot}	CH ₃ O(OH)NO ₂ conformer 2	TS _{4c}	$\Delta(RX)$
M06-2X/6-31+G**	30.86	21.67	23.53	20.16	28.48	-7.32
UCCSD(T*)-F12a/VTZ-F12	31.95	25.56	27.22	23.74	30.44	-6.47
UCCSD(T*)-F12b/VTZ-F12	32.06	25.68	27.35	23.86	30.54	-6.51
UCCSD(T*)-F12a/VQZ-F12	32.15	25.58	27.24	23.74	30.58	-6.54
UCCSD(T*)-F12b/VQZ-F12	32.18	25.62	27.29	23.78	30.61	-6.56
UCCSD(T*)-F12a/CBS1	32.30	25.59	27.26	23.75	30.69	-6.60
UCCSD(T*)-F12b/CBS1	32.27	25.57	27.24	23.73	30.66	-6.59
UCCSD(T*)-F12a/CBS2	32.22	25.58	27.25	23.74	30.64	-6.57
UCCSD(T*)-F12b/CBS2	32.23	25.60	27.26	23.76	30.64	-6.57
Best ΔE_e (F12ave/CBSave) ^a	32.25(7)	25.59(3)	27.25(3)	23.74(4)	30.66(5)	-6.58(3)
$\Delta(ZPE)$	1.97	3.09	3.04	3.21	1.77	0.06
ΔE_{0K} (= best ΔE_e + ΔZPE)	34.22	28.68	30.30	26.95	32.42	-6.53
ΔE_{0K} (include SO of OH)	34.42	28.88	30.50	27.15	32.62	-6.33
ΔH_{298K}		27.44		25.76		-6.98
ΔH_{298K} (include SO of OH)		27.64		25.96		-6.78
ΔH_{298K} (using $\Delta H_{f,298K}$ values) ^b						-7.77

^a The average of four CBS values (uncertainties w.r.t. F12b/VQZ-F12 values).

^b Using $\Delta H_{f,298K}$ values of CH₃ONO₂, -29.16 kcal mol⁻¹;⁵⁰ OH, 8.93 kcal mol⁻¹;⁵¹ CH₃O, 4.1 kcal mol⁻¹;⁷⁰ HNO₃, -32.101 kcal mol⁻¹.⁶⁸

Table 6. Some major geometrical parameters (bond distance; in Å), the imaginary vibrational frequencies (ω_i ; in cm^{-1}), the ΔE_e , ΔE_{0K} (w.r.t. separate reactants; in kcal mol^{-1}) and the zero-point energy correction $\{\Delta(\text{ZPE})$; in kcal mol^{-1} \} of the three TS's in the $\text{OH} + \text{CH}_3\text{ONO}_2 \rightarrow \text{H}_2\text{O} + \text{CH}_2\text{ONO}_2$ channel.

ΔE_e (in kcal mol^{-1})	TS _{1a}	TS _{1b}	TS _{1c}
ω_i^a	1294i	1135i	1486i
C···H bond distance	1.20	1.19	1.22
H···O bond distance	1.33	1.36	1.29
$L = \Delta(\text{C-H})/\Delta(\text{H-O})$	0.39	0.25	0.39
M06-2X/6-31+G**	3.01	5.10	6.23
UCCSD(T*)-F12a/VTZ-F12	3.88	5.39	6.94
UCCSD(T*)-F12b/VTZ-F12	3.88	5.39	6.93
UCCSD(T*)-F12a/VQZ-F12	3.98	5.48	7.01
UCCSD(T*)-F12b/VQZ-F12	3.97	5.47	7.00
UCCSD(T*)-F12a/CBS1	4.04	5.55	7.06
UCCSD(T*)-F12b/CBS1	4.03	5.53	7.05
UCCSD(T*)-F12a/CBS2	4.01	5.51	7.04
UCCSD(T*)-F12b/CBS2	4.00	5.50	7.03
Best ΔE_e (F12ave/CBSave) ^b	4.02	5.52	7.05
$\Delta(\text{ZPE})^c$	-1.46	-1.70	-2.20
ΔE_{0K} (= best $\Delta E_e + \Delta\text{ZPE}$)	2.56	3.82	4.84
ΔE_{0K} (include SO of OH) ^d	2.76	4.02	5.04

^a Computed at the M06-2X/6-31+G** geometries.

^b The average of four CBS values (uncertainties w.r.t. F12b/VQZ-F12 values).

^c Using computed M06-2X/6-31+G** harmonic frequencies.

^d Including spin-orbit splitting in OH ($0.40 \text{ kcal mol}^{-1} = 0.0006 \text{ Hartree}$), the $^2\Pi_{3/2}$ SO state of OH is lower than the unperturbed $^2\Pi$ state by $0.20 \text{ kcal mol}^{-1}$.

Table 7. Computed ΔE_e , ΔE_{0K} and ΔH_{298K} (w.r.t. separate reactants; in kcal mol⁻¹) of various species in the out-of-plane OH + CH₃ONO₂ → H₂O + CH₂ONO₂ channel 1(a) obtained at various UCCSD(T*)-F12x//M06-2X/6-31+G** levels of calculations.

ΔE_e (in kcal mol ⁻¹)	RC _{1a}	TS _{1a}	PC _{1a}	$\Delta(RX)$
M06-2X/6-31+G**	-5.41	3.01	-20.34	-14.63
UCCSD(T*)-F12a/VTZ-F12	-3.05	3.88	-20.34	-17.02
UCCSD(T*)-F12b	-3.03	3.88	-20.34	-17.02
UCCSD(T*)-F12a/VQZ-F12	-3.02	3.98	-20.46	-17.16
UCCSD(T*)-F12b	-3.02	3.97	-20.45	-17.15
UCCSD(T*)-F12a/CBS1 ^a	-3.00	4.04	-20.54	-17.27
UCCSD(T*)-F12b/CBS1 ^a	-3.01	4.03	-20.53	-17.24
UCCSD(T*)-F12a/CBS2 ^b	-3.01	4.01	-20.50	-17.21
UCCSD(T*)-F12b/CBS2 ^b	-3.02	4.00	-20.49	-17.20
Best ΔE_e (F12ave/CBSave) ^c	-3.01(1)	4.02(5)	-20.51(7)	-17.23(8)
$\Delta(ZPE)^d$	1.11	-1.46	-0.03	-1.31
ΔE_{0K} (= best ΔE_e + ΔZPE)	-1.91	2.56	-20.54	-18.54
ΔE_{0K} (include SO of OH) ^e	-1.71	2.76	-20.34	-18.34
Experimentally derived ΔE^\ddagger		1.20 ^f 2.03 ^g		
ΔH_{298K}	-1.94	1.62	-20.00	-18.10
ΔH_{298K} (include SO of OH) ^e	-1.74	1.82	-19.80	-17.90
ΔH_{298K} (using $\Delta H_{f,298K}$ values)				-13.92, ^h -17.72 ⁱ

^a Using the $1/X^3$ CBS extrapolation of the ΔE_e at the UCCSD(T*)-F12/VTZ-F12 and UCCSD(T*)-F12/VQZ-F12 levels.

^b Using the generalized two point CBS expression of Schwenke³⁸ $\{E_{CBS}=(E_{large}-E_{small})F+E_{small}$, with $F = 1.363388$ from Hill et al.³⁹ $\}$ with the UCCSD(T*)-F12/VTZ-F12 and VQZ-F12 values.

^c The best CBS estimate is the average of all the four CBS values and the estimated uncertainties are the differences between the best estimates and the UCCSD(T*)-F12b/VQZ-F12 values.

^d Using computed M06-2X/6-31+G** harmonic frequencies.

^e Including spin-orbit splitting in OH (0.40 kcal mol⁻¹ = 0.0006 Hartree), the ²Π_{3/2} SO state of

1
2
3 OH is lower than the unperturbed $^2\Pi$ state by $0.20 \text{ kcal mol}^{-1}$.
4

5 ^f Determined experimentally in Ref. [15].
6

7 ^g Determined experimentally in Ref. [14].
8

9 ^h Using $\Delta H_{f,298K}$ values of CH_3ONO_2 , $-29.16 \text{ kcal mol}^{-1}$; ⁵⁰ OH, $8.93 \text{ kcal mol}^{-1}$; ⁵¹ CH_2ONO_2 ,
10 $23.65 \text{ kcal mol}^{-1}$; ⁵⁰ H_2O , $-57.7978 \text{ kcal mol}^{-1}$. ⁵²
11

12 ⁱ Using the $\Delta H_{f,298K}$ values of -29.71 and $19.30 \text{ kcal mol}^{-1}$ for CH_3ONO_2 and CH_2ONO_2
13 respectively, which were computed in our previous study,¹¹ instead of the values from
14 Burcat⁵⁰ given in footnote (f).
15
16
17
18
19
20
21
22
23
24
25
26
27
28
29
30
31
32
33
34
35
36
37
38
39
40
41
42
43
44
45
46
47
48
49
50
51
52
53
54
55
56
57
58
59
60

Table 8.

Comparison of computed $k^{\text{ICVT/SCT}}$ values $\{\text{cm}^3 \text{ molecule}^{-1} \text{ s}^{-1}; k^{\text{ICVT/SCT}} = 2k(1a) + 2k(1b) + k(1c)\}$ of the $\text{OH} + \text{CH}_3\text{ONO}_2 \rightarrow \text{H}_2\text{O} + \text{CH}_2\text{ONO}_2$ reaction (column 2 and 3) at different temperatures obtained with the HL UCCSD(T*)-F12ave/CBSave//M06-2X IRC and available experimental values. Column 3 obtained with ΔE_e^\ddagger values 4.22 (1a), 5.72 (1b) and 7.25 (1c) kcal.mol^{-1} and column 2 obtained with these values reduced by 2.5 kcal.mol^{-1} (see text).

T (K)	$k_{\text{ICVT/SCT}}$	$k_{\text{ICVT/SCT}}$	Nielsen ^a	Kerr ^b	Gaffney ^c	Talukdar ^d	Kakesu ^e	Shallcross ^f
200	9.98E-15	9.07E-17						
220	1.38E-14	1.70E-16						
221						8.12E-15		
225						8.81E-15		
240	1.88E-14	3.04E-16						
250						1.39E-14		
260	2.52E-14	5.20E-16						
275						2.01E-14		
280	3.32E-14	8.55E-16						
290								
298	4.19E-14	1.29E-15	2.99E-13		3.40E-14			5.40E-14
300	4.29E-14	1.35E-15	2.93E-13			2.74E-14		5.48E-14
303				3.70E-13				
304							3.00E-14	
320	5.47E-14	2.06E-15						
325			2.23E-13			3.56E-14		6.39E-14
340	6.87E-14	3.06E-15						
350			1.77E-13			4.45E-14		7.30E-14
358								
360	8.52E-14	4.40E-15						
375			1.45E-13			5.40E-14		8.19E-14
380	1.04E-13	6.17E-15						
393			1.28E-13					
400	1.26E-13	8.47E-15				6.41E-14		9.06E-14
414						6.98E-14		
423								9.84E-14

^a From Ref. [18]; rate coeffs. calculated from Arrhenius expression provided

^b From Ref. [19].

^c From Ref. [16].

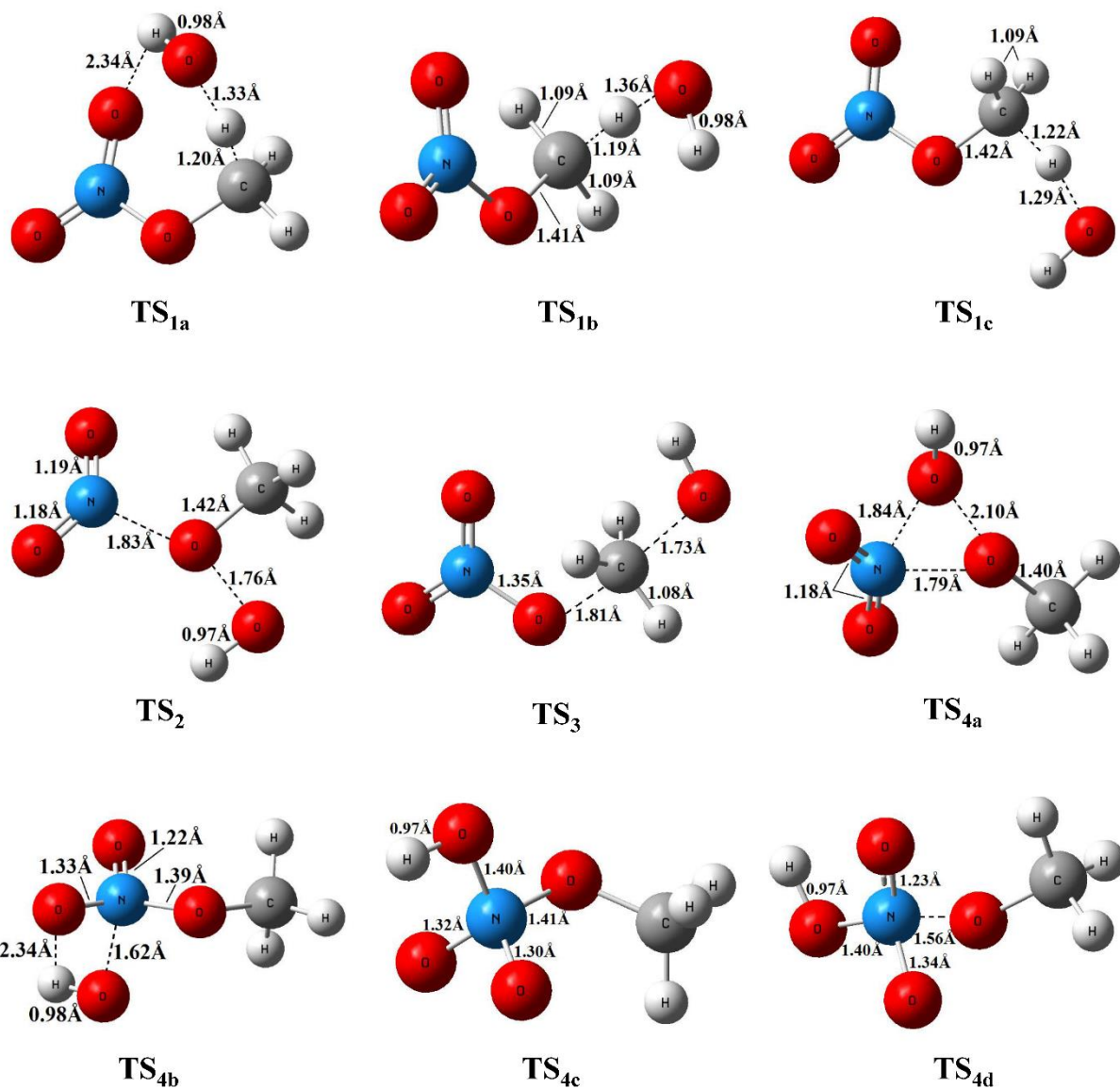
^d From Ref. [14]; rate coeffs. calculated from Arrhenius expression provided

^e From Ref. [17];

^f From Ref. [15]; rate coeffs. calculated from Arrhenius expression provided

1
2
3
4
5
6
7
8
9
10
11
12
13
14
15
16
17
18
19
20
21
22
23
24
25
26
27
28
29
30
31
32
33
34
35
36
37
38
39
40
41
42
43
44
45
46
47
48
49
50
51
52
53
54
55
56
57
58
59
60

Figure 1. Optimized geometries of the TS's at the M06-2X/6-31+G** level.



1
2
3
4
5
6
7
8
9
10
11
12
13
14
15
16
17
18
19
20
21
22
23
24
25
26
27
28
29
30
31
32
33
34
35
36
37
38
39
40
41
42
43
44
45
46
47
48
49
50
51
52
53
54
55
56
57
58
59
60

Figure 2. Optimized geometries of the adduct conformers in channel (4) and the complexes associated with TS_{1a} in channel (1) at the M06-2X/6-31+G** level. The reaction complexes through TS_{1a} , TS_{1b} and TS_{1c} have been optimised for reaction 1 and were considered in the rate coefficient calculations. Reactions 1a and 1b share the same reaction complex. For clarity only the reaction complex (RC_{1a}) is shown in this figure.

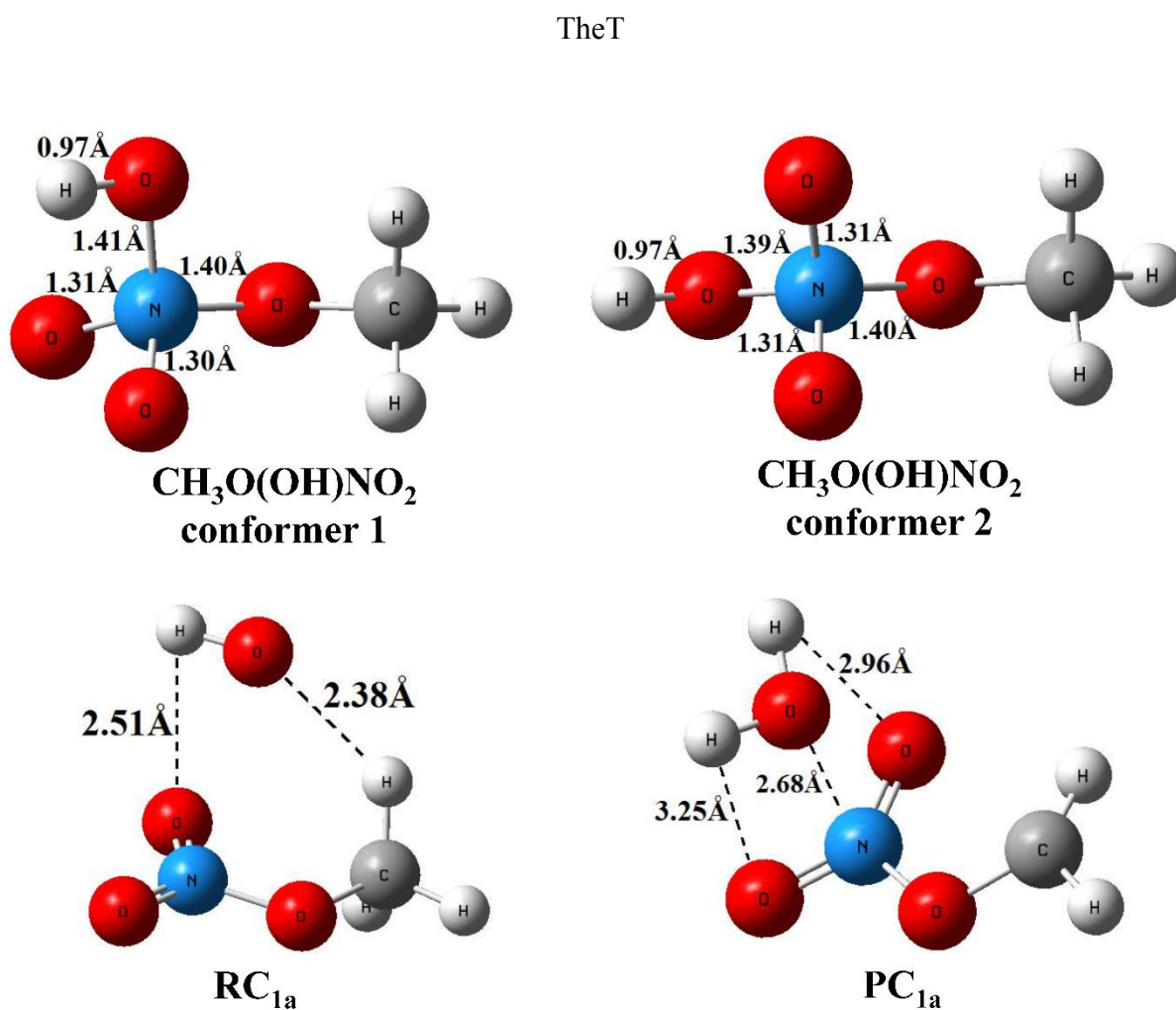


Figure 3. A schematic potential energy surface of the OH + CH₃ONO₂ reaction at the UCCSD(T*)-F12ave/CBSave//M06-2X level, including the ZPE and the SO corrections.

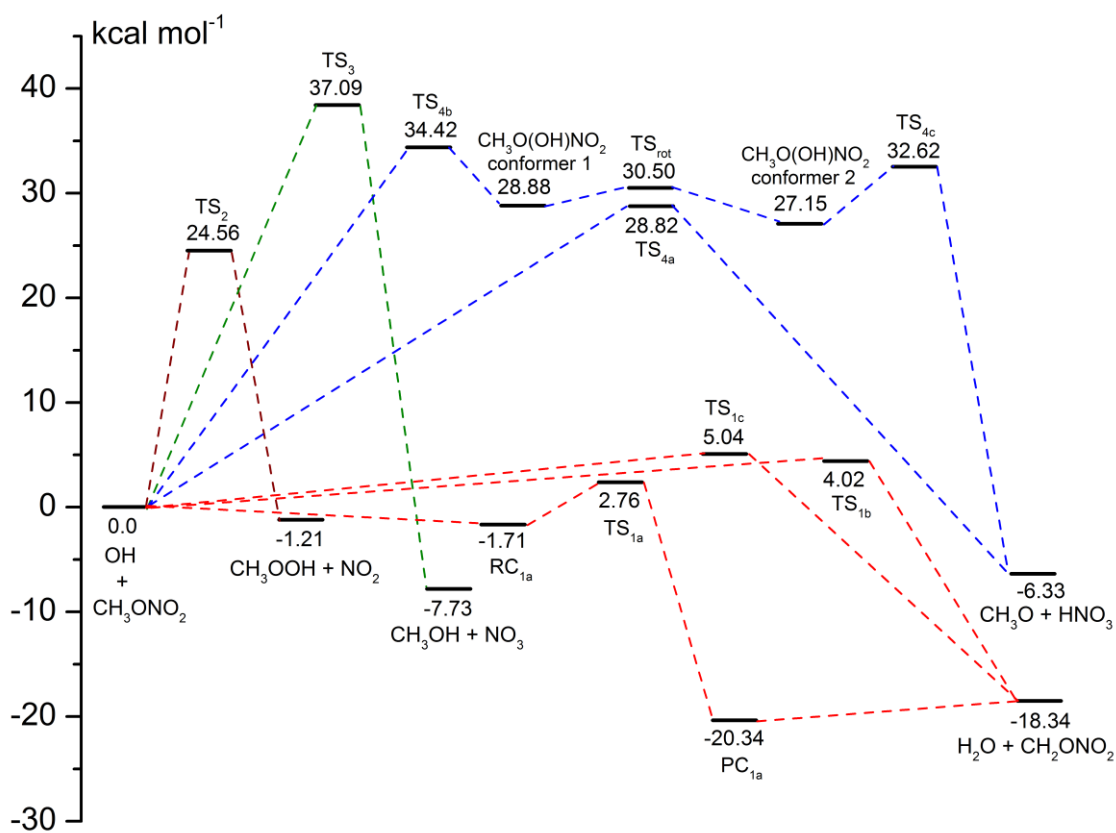


Figure 4. V_{MEP} , ΔZPE and V_{a}^{G} curves of the M06-2X/6-31+G** level (top) and the F12ave/CBSave//M06-2X level (bottom) for the out-of-plane OH + CH₃ONO₂ → H₂O + CH₂ONO₂ channel via TS_{1a}. The higher level (HL) V_{MEP} and V_{a}^{G} curves (bottom) were obtained by using the HL energies of the reactants, RC_{1a}, TS_{1a}, PC_{1a} and products, with more HL IRC points calculated by the expression devised by us previously (see text).⁴⁹

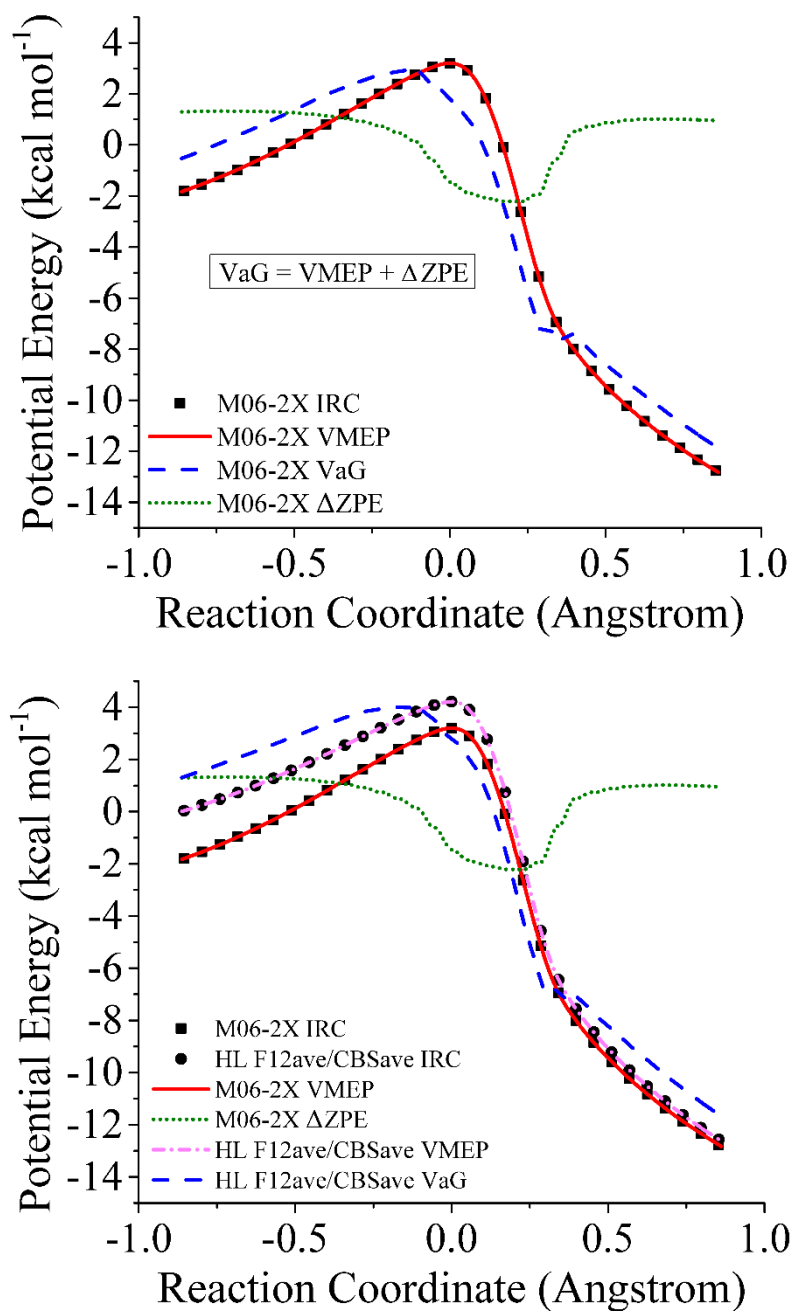


Figure 5. Computed rate coefficients (k ; in $\text{cm}^3 \text{molecule}^{-1} \text{s}^{-1}$) for the $\text{OH} + \text{CH}_3\text{ONO}_2 \rightarrow \text{H}_2\text{O} + \text{CH}_2\text{ONO}_2$ reaction (channel 1(a)) at different temperatures (T) obtained at different VTST levels using the M06-2X/6-31+G** IRC (computed k values have been multiplied by two to account for two out-of-plane H abstraction sites with hydrogen bond-like interaction).

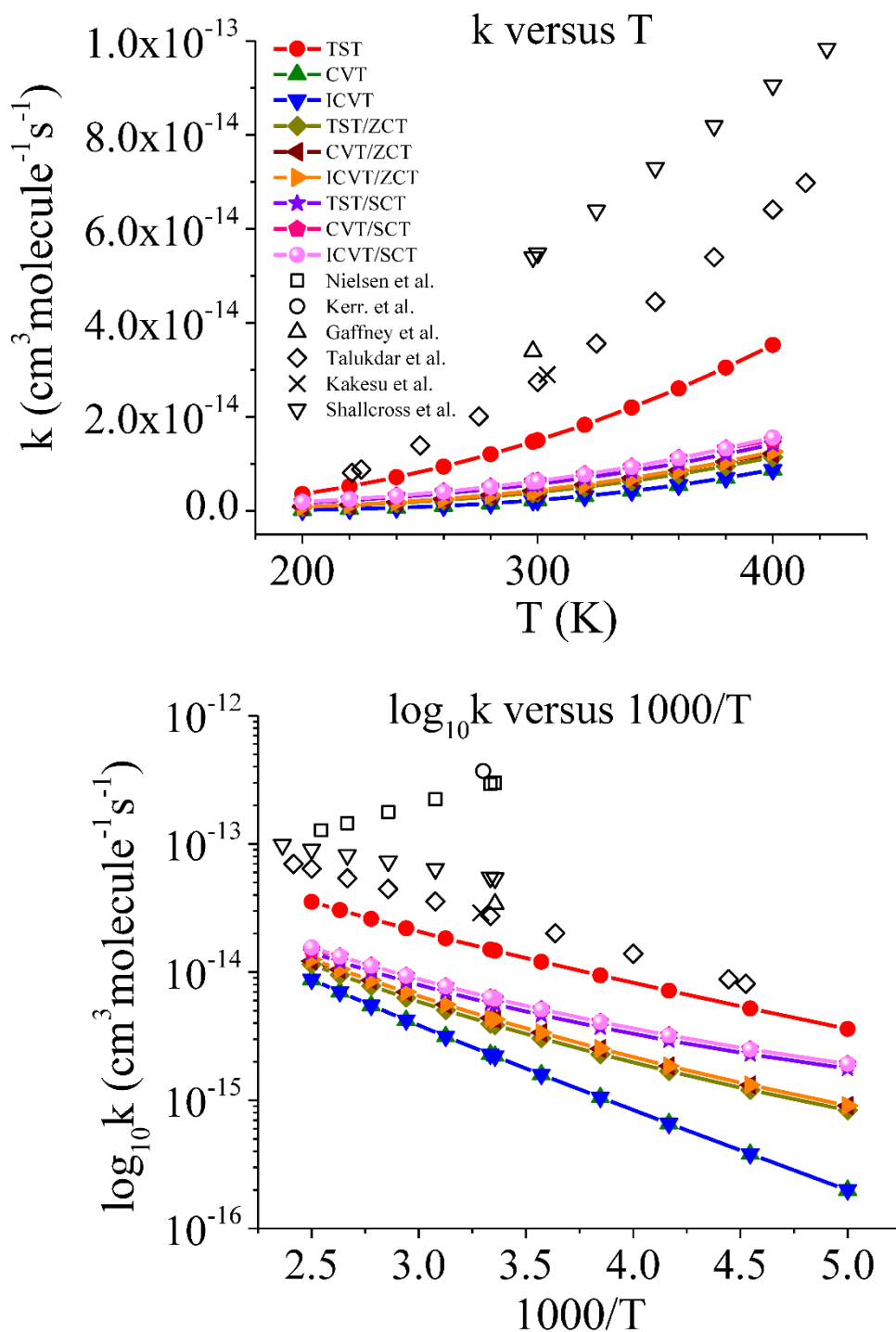


Figure 6. Rate coefficients (k ; in $\text{cm}^3 \text{molecule}^{-1} \text{s}^{-1}$) computed at different VTST levels for the $\text{OH} + \text{CH}_3\text{ONO}_2 \rightarrow \text{H}_2\text{O} + \text{CH}_2\text{ONO}_2$ reaction (reaction 1(a)) with the HL F12ave/CBSave//M06-2X/6-31+G** IRC in the temperature range between 200 K and 400 K (computed k values have been multiplied by two to account for two H abstraction sites with hydrogen bond).

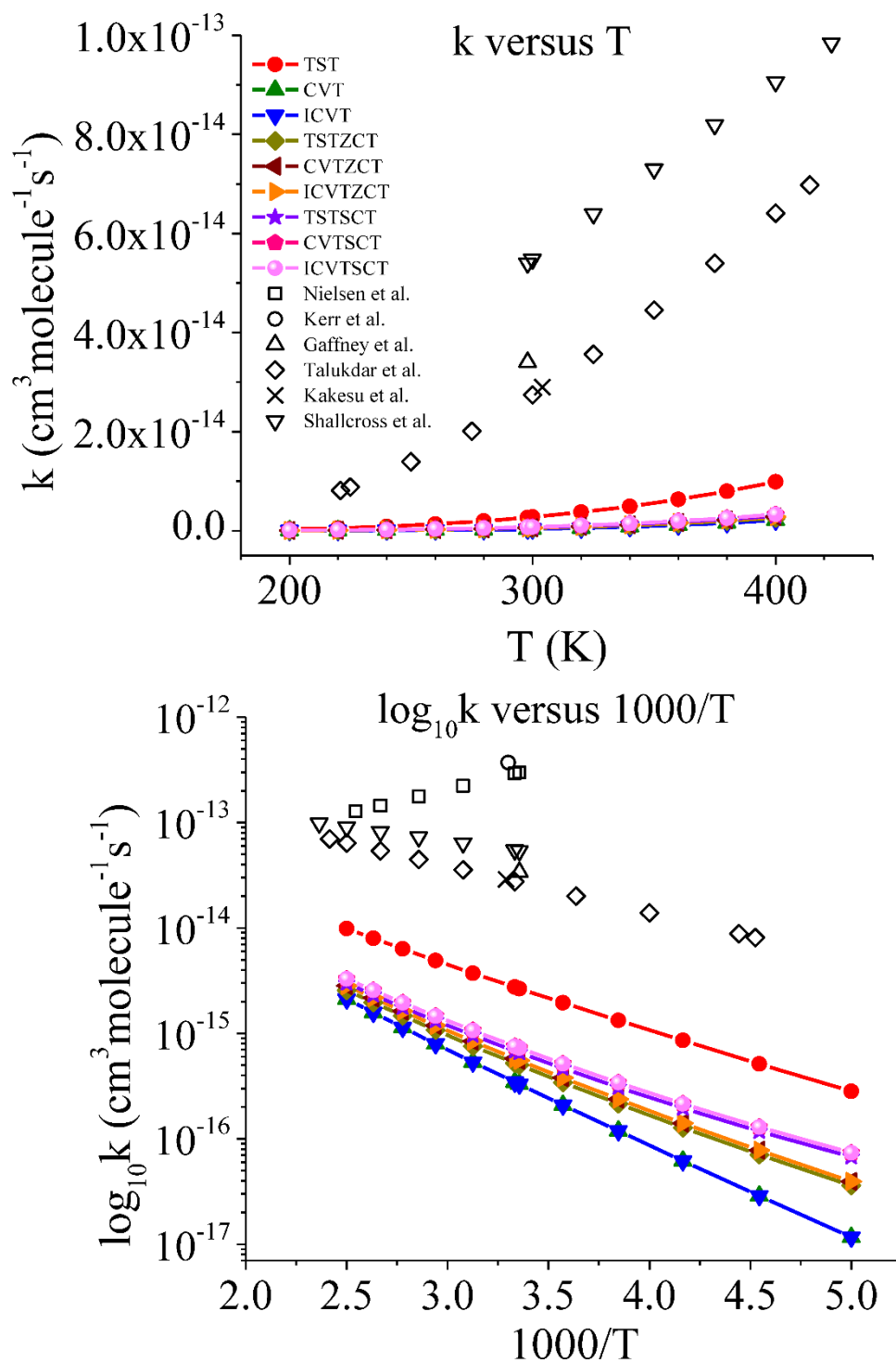
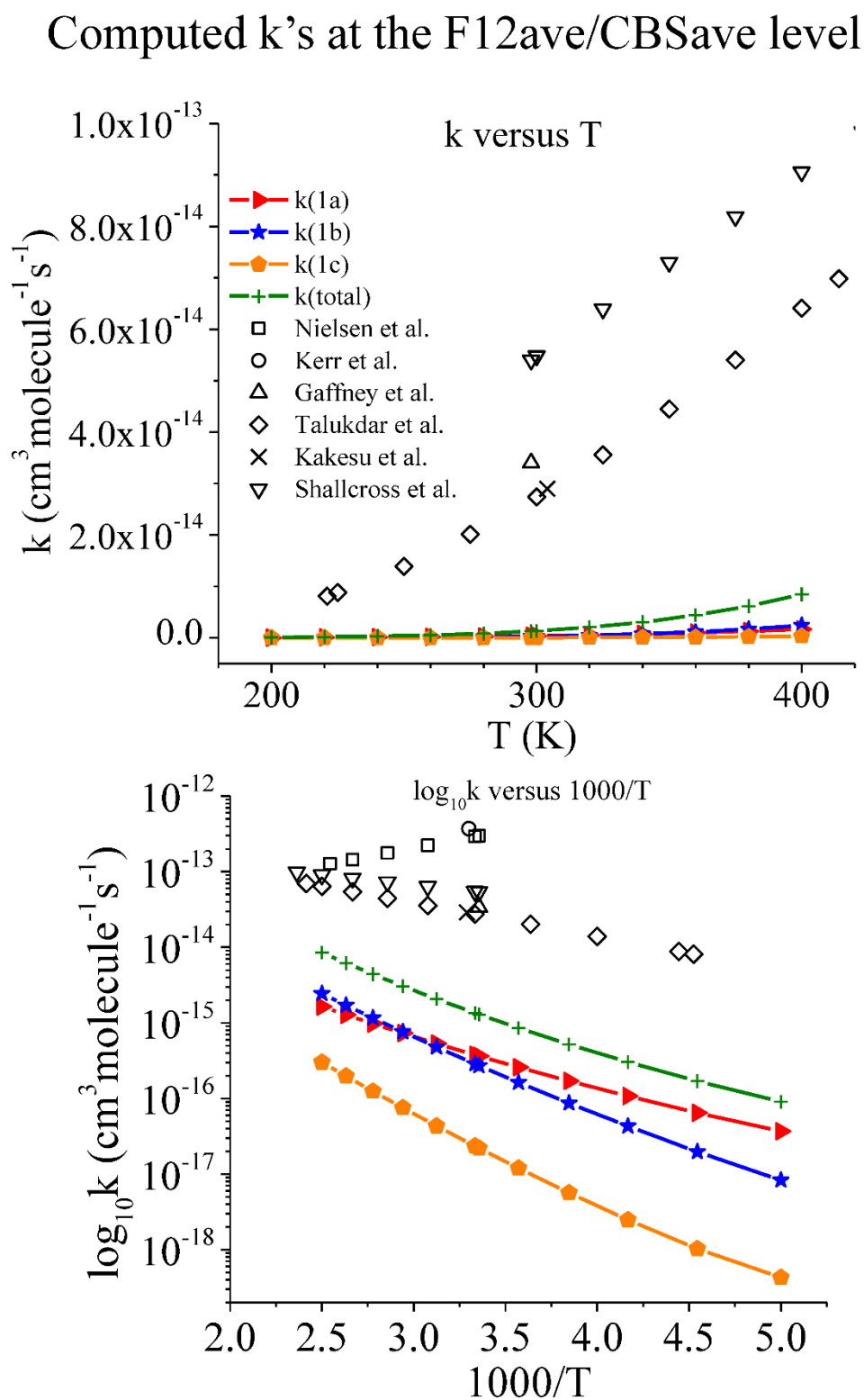
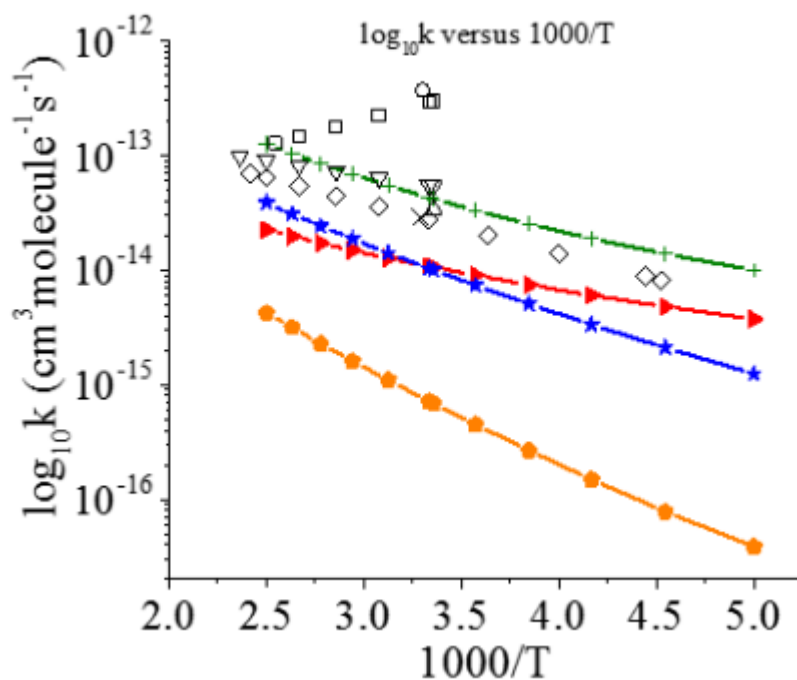
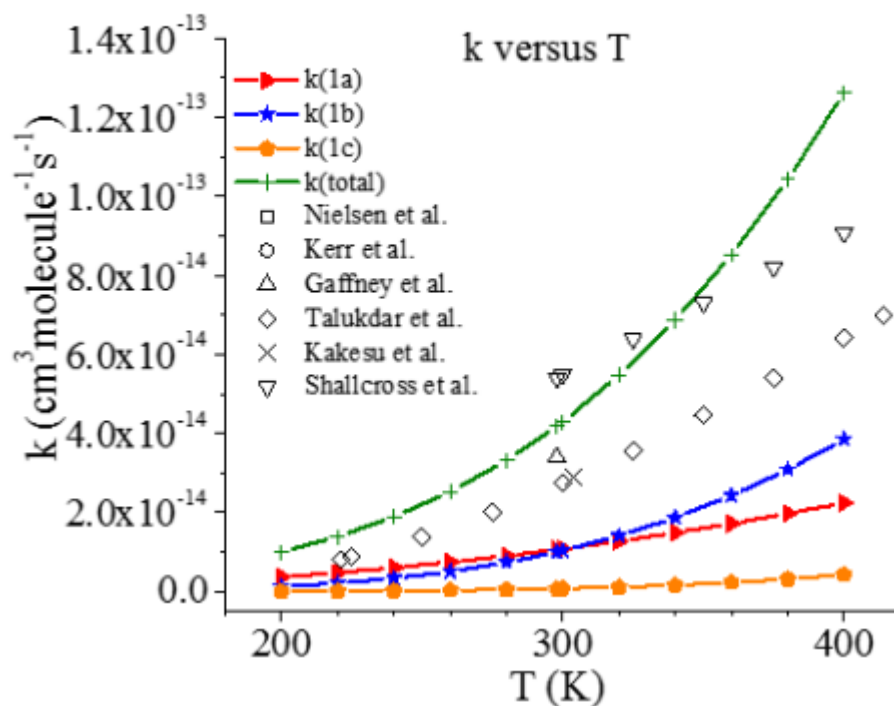


Figure 7. Computed ICVT/SCT rate coefficients (k ; in $\text{cm}^3 \text{molecule}^{-1} \text{s}^{-1}$) of reactions (1a), (1b) and (1c), as well as the total rate coefficients of the $\text{OH} + \text{CH}_3\text{ONO}_2 \rightarrow \text{H}_2\text{O} + \text{CH}_2\text{ONO}_2$ reaction with the HL F12ave/CBSave//M06-2X/6-31+G** IRC in the temperature range between 200 K and 400 K $\{k(\text{total}) = 2k(1a) + 2k(1b) + k(1c)\}$.



1
2
3
4 **Figure 8** Computed ICVT/SCT rate coefficients (k ; in $\text{cm}^3 \text{ molecule}^{-1} \text{ s}^{-1}$) of reactions (1a),
5 (1b) and (1c), as well as the total rate coefficients of the $\text{OH} + \text{CH}_3\text{ONO}_2 \rightarrow \text{H}_2\text{O} +$
6 CH_2ONO_2 reaction with the HL F12ave/CBSave//M06-2X/6-31+G** IRC in the temperature
7 range between 200 K and 400 K $\{k(\text{total}) = 2k(1a) + 2k(1b) + k(1c)\}$, with the HL
8 F12ave/CBSave//M06-2X/6-31+G** barrier heights for channels 1(a), 1(b) and 1(c) reduced
9 by $2.5 \text{ kcal.mol}^{-1}$ (see text).
10
11
12
13
14
15
16
17
18
19
20
21
22
23
24
25
26
27
28
29
30
31
32
33
34
35
36
37
38
39
40
41
42
43
44
45
46
47
48
49
50
51
52
53
54
55
56
57
58
59
60

Computed k 's at the F12ave/CBSave level

TOC GRAPHIC

